

Fabrication of Protein Arrays Using Electron Beam Lithography

Thesis submitted to
The Graduate College of
Marshall University

In partial fulfillment of the
Requirements for the Degree of
Master of Science
Chemistry

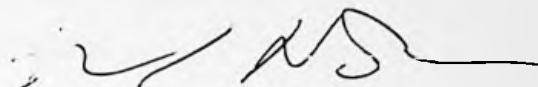
By
Duy-Bao Phan Dinh

Marshall University
Huntington, West Virginia

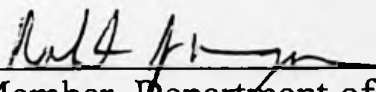
August 11, 1999

Marshall University
Department of Chemistry

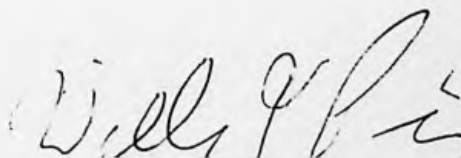
THIS THESIS WAS ACCEPTED ON August 11, 1999
AS MEETING THE RESEARCH REQUIREMENTS FOR THE
DEGREE OF MASTER OF SCIENCE



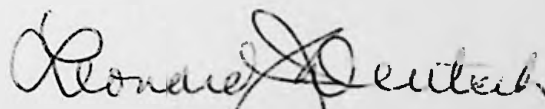
Advisor, Department of Chemistry



Member, Department of Chemistry



Member, Department of Chemistry



Dean, Graduate School

Acknowledgments

To My Dad, My Mom, My Sister, and All My Friends,
Thank You for Making This and Every Day Possible.

Acknowledgements

I would like to give a special thanks to Dr. Michael (Micro) Norton for being my advisor and pulling me through the thorns of research. I would also like to thank Dr. William Price, Dr. Robert Morgan for being on my committee and Dr. Todd Green at the medical school for helping with my understanding of cell biology. Thanks to all the professors and staffs of the chemistry department at Marshall University for being good friends.

Table of Contents:

	Page
List of Figures	iv
List of Tables.....	vi
Abstract	vii
I. Introduction	1
A. <u>The History of Micro-patterning of Protein Films</u>	1
B. <u>The Importance of Patterning Proteins</u>	2
C. <u>Different Micro-Patterning Techniques</u>	3
1. <i>Photoresist Technology</i>	6
2. <i>Photochemical Technology</i>	9
3. <i>Self-Assembled Monolayer(SAM)</i>	11
D. <u>Laminin</u>	12
E. <u>Scanning Electron Microscopy (SEM)</u>	17
F. <u>Confocal Microscopy</u>	18
II. Project Goal	20
III. Hypothesis	20
A. <i>Estersils</i>	22
IV. Instrumentation	24

V. Materials	24
VI. Experimental: Standard Methods	25
A. <i>Flame Drying</i>	25
B. <i>Dichlorodimethylsilane Treatment</i>	25
C. <i>Laminin Treatement</i>	26
D. <i>Primary Antibody Treatment</i>	26
E. <i>Secondary Antibody (FITC) Treatment</i>	26
F. <i>Mounting of Coverslip</i>	27
G. <i>Standard SEM Parameters: Masked Exposure</i>	27
H. <i>Preparation of Coverslip for Observation under the Confocal</i>	27
I. <i>Standard Confocal Parameters</i>	28
J. <i>Quantitation of Intensities</i>	28
VII. Experiments: Results and Discussions	29
A. <i>Nickel Mask Experiment</i>	31
1. Dichlorodimethylsilane Treatment before Electron Irradiation (Sample A)	31
2. Electron Irradiation after Protein Treatment (Sample B)	37
3. Electron Irradiation before Protein Treatment (Methanol Flame Dried) (Sample C)	41
4. Repeated Electron Irradiation before Protein Treatment (Sample D)	45
5. Electron Irradiation before Protein Treatment (Ethanol Flame Dried) (Sample E)	48
6. Blank Experiment without Methanol (Sample F)	52
7. Blank Experiment with Methanol (Sample G)	55
B. <i>Maskless Experiments</i>	58
1. Testing a Program for Generating Patterns by Electron Beam Direct Write Using a KBr Crystal (Sample H)	58
2. Electron Beam Direct Write on Coverslip (Sample I)	60
3. Testing A New Program to Investigate Irradiation Time Dependence Using a KBr Crystal (Sample J)	63
4. Time of Exposure Versus Intensity without antibody (Sample K)	65
5. Treating Sample K with FITC antibody (Sample L)	69

6. Short (One-Second) Electron Irradiation of Coverslip Under the Nickel Grid (Without Antibody) Sample M	73
--	----

VIII. Summary and Conclusion.....	77
--	-----------

IX. Future Experiments.....	78
------------------------------------	-----------

X. Appendix A	79
----------------------------	-----------

XI. References.....	82
----------------------------	-----------

List of Figures

Figure 1. Percent Apoptosis as a Function of Confinement.....	3
Figure 2. Diagram for Preparing Pattern Surface Using Photoresist Technology	7
Figure 3. Patterns Observed by Photoresist Technology	8
Figure 4. One Scenario for Photochemical Protein Patterning	10
Figure 5. Diagram of SAM Preparation	11
Figure 6. Molecular Structure of Basal Laminin.....	13
Figure 7a. The Three Different Ways Basal Laminae Organize	14
Figure 7b. Electron Micrograph of Basal Laminin	15
Figure 8. Schematic of Laminin.....	16
Figure 9. Basic Working of Confocal Microscope	19
Figure 10. Schematic Diagram of Process of Producing Protein Patterns	21
Figure 11a. The Two Types of End Groups on the Surface of Glass, Silanol and Siloxane	22
Figure 11b. Methanol Reacting with Glass Surface.....	23
Figure 12a. SEM Micrograph of the Nickel Grid	29
Figure 12b. SEM Micrograph at the Edge of the Circular Hole of the Nickel Grid.....	30
Figure 13. Reaction of Dichlorodimethylsilane with the Surface of Glass.....	32
Figure 14. Bond Breaking Due to Electron Bombardment, Allowing for Protein Adhesion.....	34
Figure 15. Confocal Micrograph of Sample A.....	35

Figure 16. Line Intensity of Sample A	36
Figure 17. Confocal Micrograph of Sample B	38
Figure 18. Line Intensity of Sample B	39
Figure 19. Exposed SiO-CH ₃ Bonds are Broken.....	42
Figure 20. Confocal Micrograph of Sample C	43
Figure 21. Line Intensity of Sample C	44
Figure 22. Confocal Micrograph of Sample D.....	46
Figure 23. Line Intensity of Sample D	47
Figure 24. Confocal Micrograph of Sample E	49
Figure 25. Line Intensity of Sample E	50
Figure 26. Confocal Micrograph of Sample F	53
Figure 27. Line Intensity of Sample F.....	54
Figure 28. Confocal Micrograph of Sample G.....	56
Figure 29. Line Intensity of Sample G.....	57
Figure 30. Electron Beam Direct Write Pattern on a KBr Crystal	59
Figure 31. Confocal Micrograph of Sample I	61
Figure 32. NiO Photoluminescence Spectra (excitation = 280 nm).....	62
Figure 33. Electron Beam Direct Write Pattern on a KBr Crystal used to Check DACTA program.....	64
Figure 34. Confocal Micrographs of Sample K	64
Figure 35. Line Intensity of Sample K.....	68
Figure 36. Confocal micrographs of Sample L	70
Figure 37. Line Intensity of Sample L	71
Figure 38a. Confocal Micrograph of Sample M	74

Figure 38b. Confocal Micrograph of Sample M, with increase in Contrast 75

Figure 39. Line Intensity of Sample M 76

List of Tables

Table 1. Different Protein Patterning Technologies 5

Table 2. Average Intensities for Sample A..... 37

Table 3. Average Intensities for Sample B 40

Table 4. Average Intensities for Sample C..... 45

Table 5. Average Intensities for Sample D..... 48

Table 6. Average Intensities for Sample E..... 51

Table 7. Average Intensities for Sample F 55

Table 8. Average Intensities for Sample G 58

Table 9. Average Intensities for Sample K 69,72

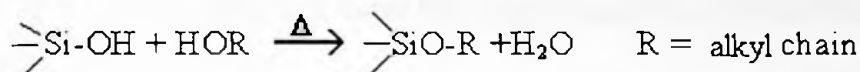
Table 10. Average Intensities for Sample L..... 72

Table 11. Average Intensities for Sample M..... 77

Abstract:

Very few electron beam based methods for producing high-resolution patterns of surface bound proteins on glass have been developed.

There are only two types of end groups at the surface of glass, they are silanol and siloxane groups. An estersil layer can be formed on the surface of glass by treatment with hot alcohol creating a hydrophobic layer. The reaction is depicted as follows.



The proposal that protein arrays could be fabricated by patterned electron bombardment using estersils as a negative resist was tested in this research. The hydrophobic estersil layer was expected to have a lower affinity to protein adhesion compared to the glass surface (silanol). Breakage of the estersil bond will expose the underlying glass surface for adhesion.

A JEOL JSM-5310LV scanning electron microscope (SEM) was used as the electron source for irradiation of coverslips. Laminin was the protein used for these patterning experiments. The rabbit polyclonal to laminin primary antibody and the goat anti-rabbit conjugated to fluorescein isothiocyanate (FITC) secondary antibody were used to identify the localization of laminin. A Bio-Rad MRC-1024 confocal microscope was used to capture micrographs of the experiments.

Several experiments, performed using a nickel grid as a mask, supported this estersil resist hypothesis. However, when control experiments were conducted using an electron beam direct write (EBDW) maskless technique, the data disclosed a more complex mechanism of adsorption. Since the only variable removed in the EBDW experiments was the mask, it was possible to evaluate the contribution of the mask to the observed adhesion. It was concluded that sputtering of the nickel mask made a significant contribution to protein adsorption.

Two viable methods for high-resolution protein patterning using electron beam methods have been devised and investigated. Both methods warrant further development for use in cellular growth regulatory projects.

Introduction:

The History of Micro-patterning of Protein Films.

The immobilization of biologicals had its beginning in 1916 when Nelson and Griffin immobilized invertase onto charcoal and alumina.^{1,2} Invertase is an enzyme sucrase that catalyzes the hydrolysis of sucrose to glucose and fructose.³ The activity of invertase was found not to be affected when adsorbed to a solid like charcoal, or to a colloid like saponin, serum, or egg albumin. Therefore, invertase may be removed from an aqueous solution by adsorption to a solid.² Since then, the technology of immobilization of biologicals to a variety of solid supports has become widely used.¹

Micropatterning of proteins is possible because of the ability to immobilize biologicals to a variety of solid supports. In 1978 MacAlear and Wehrung used photoresist technology from the semiconductor industry to create patterns onto an underlying compressed protein layer.⁴ This was accomplished by dispensing with an eyedropper, the premade solution of phosphatase in liquid monomer (made from 90 parts by volume of butyl methacrylate and 10 parts by volume of methyl methacrylate), onto a silicon wafer. This film can be characterized as a solid matrix of copolymerized polybutyl methacrylate and polymethyl methacrylate with the phosphatase evenly distributed.

One example of creating patterns using such a thin film employed electron irradiation of the film by a computer-controlled electron microscope and, tracing the negative of the desired micropattern on the polymeric film. As a result, the polymeric material in the area traced by the

beam is depolymerized and the phosphatase contained therein is completely deactivated. The substrate is then treated with both creatinine phosphate and lead nitrate. The remaining active phosphatase breaks down the creatinine phosphate into creatinine and phosphate. The lead nitrate then reacts with the liberated phosphate producing lead phosphate. Finally, the wafer was baked in an oven for 5 hours at 320°C , under non-oxidizing conditions to reduce the lead phosphate to metallic lead in the positive areas and to destroy all of the polymeric material. The elemental lead produced is deposited on the silicon dioxide film as a conductive body extending throughout the positive area of the micropattern, the negative area being constituted of exposed portions of the silicon dioxide film. The patterns obtained satisfied their objective of producing metallic micropatterns without depending on vacuum deposition. These patterns were intended for creating a bio-electronic microcircuit.⁵ After that, there has been a growth of research in the area of protein patterning.⁴

The Importance of Patterning Proteins.

Patterning proteins confers many advantages. One example is that patterned surfaces provide novel ways to study a wide variety of cellular activities under highly controlled conditions.^{6,7} For example, Ingber et al. have demonstrated the ability to control the life of human and bovine capillary endothelial cells by controlling the area of the substrate on which they were grown. It was found that cells are more likely to enter the apoptosis (programmed cell death) stage when confined to a patterned surface with a diameter of $10\text{-}\mu\text{m}$ than when confined to a $20\text{-}\mu\text{m}$ diameter surface. Figure 1 shows the percentage of apoptosis for the suspended cells, the cells in $10\text{-}\mu\text{m}$ and $20\text{-}\mu\text{m}$ confinement, and that of the unrestricted cells.

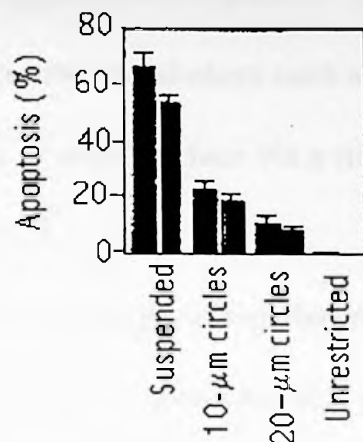


Figure 1. Percent Apoptosis as a Function of Confinement.⁷

The suspended cells have the highest percentage going to apoptosis while the unrestricted cells have the lowest percentage of apoptosis. Acquiring expertise in controlling the apoptotic switch of capillary cells has great clinical implications, since angiogenesis (the ability to evoke blood vessel formation) is a precursor for tumor growth.^{7,8}

The ability to pattern proteins on solid surfaces is also important in many areas of biotechnology such as in production, storage, and delivery of pharmaceutical proteins. Furthermore, protein patterning facilitates purification of proteins by chromatography, design of biosensors, and production of supports for tissue culture.⁹

Different Micro-Patterning Techniques.

The simplest method for immobilizing protein on surfaces is physical adsorption where there is an attraction between the solid surface and the protein. A more stable means of protein

immobilization is to covalently link a protein to the surface via a chemical bond between the solid support and the protein. An example of this type of immobilization is the use of bifunctional crosslinkers such as silanes, or any silica-based linkers which can bind at one end to a glass or metal surface via a silanol bond while at the other end using a group for binding protein.¹⁰

Several protein-patterning techniques are shown in Table 1.⁴ The three major techniques are photoresist, photochemical and self-assembled monolayer (SAM).

Table 1. Different Protein Patterning Technologies⁴

Patterning Technique	Resolution	Application	Substrate
Photoresist technology with alkyl- and amino-terminated silanes	<10 μm	Controlled cellular growth	Silicon, SiO ₂
Photoresist technology with methyl- and amino-terminated silanes	<10 μm	Controlled cellular growth	Glass, fused silica
	1.5 μm	Protein immobilization and enzymatic assay	Glass, fused silica
Photoresist technology with methyl-, amino- and alkyl-terminated silanes	10 μm	Controlled cellular growth; protein immobilization	Glass, quartz
Nitroarylazide photochemistry with biotin/avidin	1.5 μm	Multiple analyte immunoassay	Gold, SiO ₂
Nitroarylazide photochemistry with RGD peptide	350 μm	Controlled cellular growth	Polyvinyl alcohol
Perfluorophenylazide photochemistry with N-hydroxysuccinimide esters	0.5 μm	Enzymatic assay	Polystyrene
Nitrobenzyl photochemistry	2.5 μm	DNA and peptide libraries	Glass
Nitrobenzyl photochemistry with biotin/streptavidin	100 μm	Immunoassay	Glass
Diazirine photochemistry with oligopeptide	300 μm	Controlled cellular growth	Polystyrene
Diazirine photochemistry with BSA/F(ab') ₂	<1 μm	Immunoassay	TiO ₂ /SiO ₂
Deep UV of silane SAMs with EDA and 13F	100 μm	Controlled cellular growth	Glass, fused silica
Deep UV of silane with OTS and EDA	1 μm	Immunoassay	SiO ₂
Deep UV of silane with OTS and EDA	100 μm	Controlled cellular growth	Glass, fused silica
Deep UV of thiol terminated silanes	25 μm	Immunoassay	Glass
UV of alkane thiol SAMs		Immunoassay	Gold
Micro-manipulation and UV lithography of alkane thiol SAMs	1 μm	Protein adsorption; controlled cellular growth	Gold
Microcontact printing of alkane thiols	10 μm	Controlled cellular growth	Gold
Electrochemical patterning of alkane thiol SAMs	10 μm	Immunoassay	Laser ablated gold on glass
UV of benzophenone alkane thiol SAMs	1 μm	Immunoassay	Gold
Laser vapor deposition of proteins	50 μm	Immunoassay	Glass
RFGD functionalization of fluoropolymers	5 μm	Controlled cellular growth	Poly(tetrafluoroethylene-co-hexa fluoropropylene
Ink-jet based robotic printing	~200 μm	DNA arrays	Glass

Photoresist Technology.

An example of photoresist technology involved using a photoresist technique on silanes to produce isolated islands to control cellular growth. Some of the initial work was performed by Kleinfeld et al., who were interested in reestablishing an ordered cytoarchitecture to nervous tissue cells by creating a patterned in vitro substrate. Similar experiments were performed by Lom et al in this area, however, EDS (N-(2-aminoethyl)-3-aminopropyl-trimethoxysilane) and DMS (dimethyldichlorosilane) were used instead of alkyl-trichlorosilane and amino-trihydroxysilane in their studies. They patterned protein (fibronectin, collagen IV, and laminin) on coverslips and visualized these patterns using a fluorescence microscope. One of their methods involved applying a layer of EDS (to prevent cell adhesion) on the coverslip followed by a layer of photoresist (Figure 2).



Figure 2. Diagram illustrating the photoresist technique for patterning silanes. The diagram shows a cross-section of a substrate with a layer of photoresist being applied over a layer of EDS (N-(2-aminoethyl)-3-aminopropyl-trimethoxysilane). The photoresist is applied in a patterned manner, creating isolated islands. The diagram is labeled with 'Photoresist' and 'EDS'.

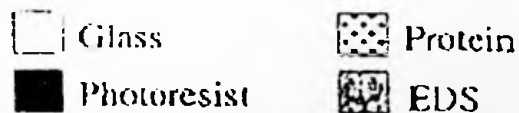
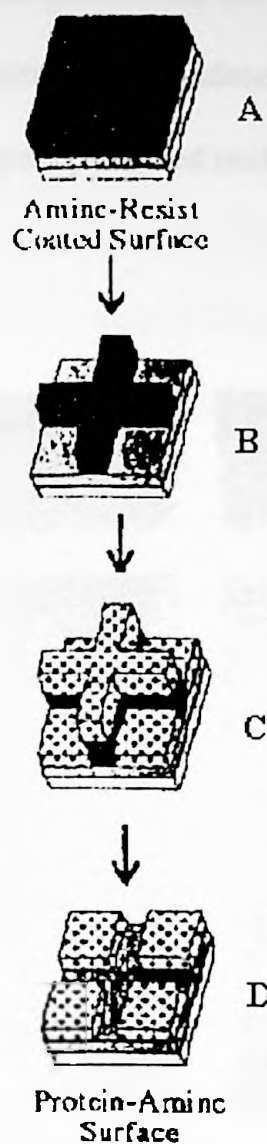


Figure 2. Diagram for Preparing a Patterned Surface Using Photoresist Technology.⁶ (A) A EDS bounded coverslip with a layer of photoresist. (B) The photoresist is lithographically define, exposing the underlying EDS layer. (C) A layer of protein is applied over the defined substrate. (D) Sonicating away the photoresist layer in acetone reveals island of protein separated by the EDS.

Then the photoresist was defined by lithography. The coverslip was then coated with protein, and the photoresist was removed by sonication in acetone revealing the underlying EDS layer. Conventional peroxidase immunostaining, created an opaque precipitate, and revealed that the proteins were patterned uniformly (Figure 3).⁶

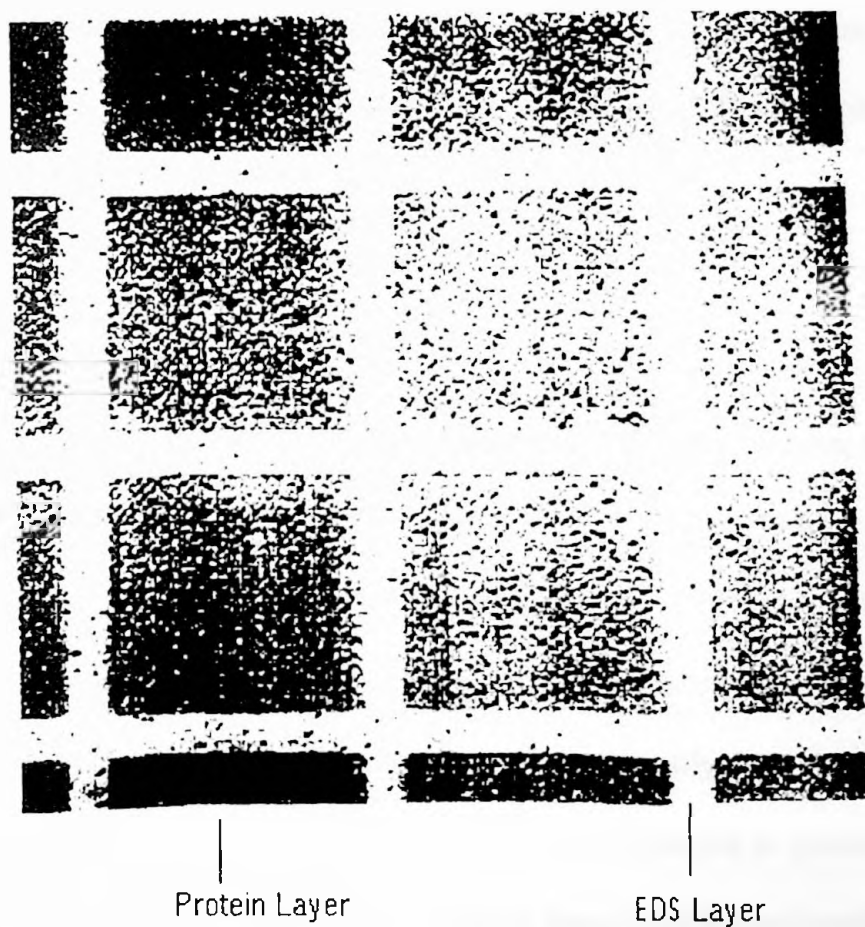


Figure 3. Patterns Observed by Photoresist Technology.⁶ Peroxidase immunostaining, created an opaque precipitate, revealed that the proteins were patterned uniformly.

The biggest advantage of photoresist-based protein patterning is that it builds upon a well-established technology. However, another advantage is the option to choose which silane will be the background silane, meaning the surface regions where protein is not bound. This allows for flexibility in varying the presented group for minimum background protein adsorption.

The most apparent disadvantage is the effect of the patterning technique on the overall protein activity. Residual solvents and photoresist can denature proteins, decreasing their activity. In addition, silanization may result in incomplete surface coverage. Incomplete coverage of the substrate could result in increased non-specific binding.^{4,11}

Photochemical Technology.

Photochemical protein patterning is another example of a two-dimensional protein patterning technique. The photochemical protein patterning method uses chemically variable species, which can be activated upon UV irradiation, to bind targeted molecules.¹² Conversely, deep UV irradiation can be used to deactivate chemical species, such as the conversion of thiol groups to sulfonates. In order to pattern protein molecules, localized areas of reactivity can be created by selectively irradiating a photochemically derivitized surface.¹⁰ One example involves a substrate derivitized with a “caged” species (similar to protecting groups). The substrate is irradiated, which removes the caging group, and leaves localized active regions on the substrate. Protein binds within the localized active regions. This process is depicted in Figure 4.¹²

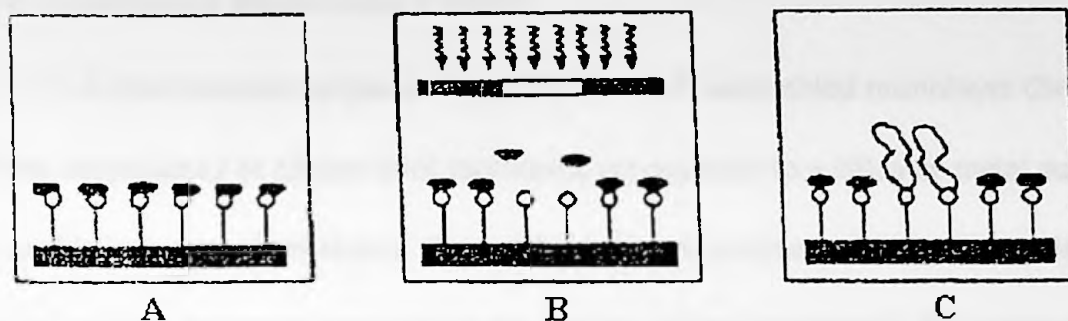


Figure 4. One Scenario for Photochemical Protein Patterning.¹² (A) A substrate derivitized with a “caged” species (similar to protecting groups). (B) The substrate is then irradiated, which removes the caging group, and leaving localized active regions on the substrate. (C) Protein binds within the localized active regions.

The benefit of photochemical methods over conventional lithographic methods is that solvents, buffers, and reactants, can be tailored to minimize the negative effect on protein activity. Most importantly, this methodology can be used repeatedly on the same surface with different proteins to create multiple protein patterns.

A concern with photochemical techniques is the limited ability to control the surface energy of the background region. The specific surface derivitization that is necessary to conduct the photochemical reaction dictates the background surface. The most difficult aspect of using photochemical methods is that the surfaces are sensitive to UV light. In order to retain maximum efficiency, the surfaces must be kept in low light until the final protein-binding step. Also, photolithographic masking must be performed via backmasking through a transparent substrate to avoid smearing of the derivitized surfaces. This may cause scatter of the irradiation source, as it must pass through the substrate of the derivitized surface.^{4,12}

Self-Assembled Monolayer (SAM).

A third method for patterning proteins is self-assembled monolayer (SAM) technology. When alkylsilanes or alkane thiol molecules are exposed to a silica or metal surface, they assemble into organized layers. One endgroup remains free to interact at the interface. Variation of the reactive endgroup can change the binding of the monolayer. By creating mixed monolayers on a surface, proteins can be patterned onto the regions of hydrophilic or adhesion promoting SAMs. Figure 5 is a schematic diagram of SAM technology, as described below.¹³

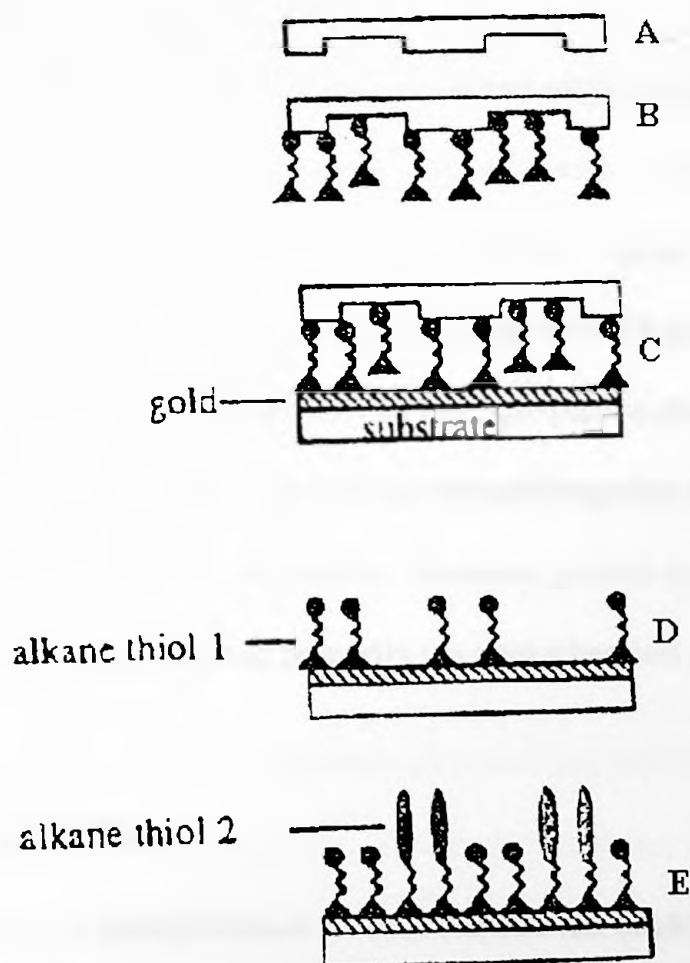


Figure 5. Diagram of SAM Preparation.¹³ (A) A stamp substrate used for SAM. (B) Stamper attached with hydrophobic alkane thiols (1). (C) Gold substrate gets stamped with alkane thiols. (D) Patterned alkane thiols adhered to gold substrate. (E) Patterned substrate immersed in a solution of hydrophilic alkane thiols (2), which adhere to unoccupied area on gold substrate with the hydrophilic endgroup ready for adhesion to protein.

Stamping of alkane thiol SAMs has been used to isolate single cells in culture. Using a prepared silicone rubber stamp, a gold surface was stamped with 10- μm grid of hexadecanethiol (thiol 1 in Figure 5). The remaining bare gold was derivitized using a solution process, with a polyethylene glycol (PEG) terminated alkanethiol, which was adhesion resistant (thiol 2 in Figure 5). When patterned surface was exposed to laminin, a protein used to attach hepatocyte cells to gold surfaces, the PEG inhibited the adsorption of laminin. Rat hepatocytes were plated onto the SAM coated gold surfaces and single-cells were cultured within the laminin controlled hexadecanethiol islands.¹³

Self-assembled monolayer techniques are useful for easily creating a monolayer with localized regions for protein immobilization. Stamping of alkane thiols has an advantage over microlithography, as the surface is never exposed to UV light. One disadvantage is that the surface is prepared ahead of time, and then the protein solution is incubated in a single step, this discourages the possibility of multiple protein patterning.^{4,13}

Overall, it appears that photolithography and SAM surfaces are the preferred methods for controlling cellular growth. However, protein patterning for immuno- or enzymatic assay has been accomplished primarily via photochemical methods.⁴

Laminin

Basal laminae are thin (40-120 nm thick) and flexible matlike regions composed of type IV collagen, heparan sulfate proteoglycan, laminin and entactin. The current model of the molecular structure of a basal lamina is shown in Figure 6.^{14,15}

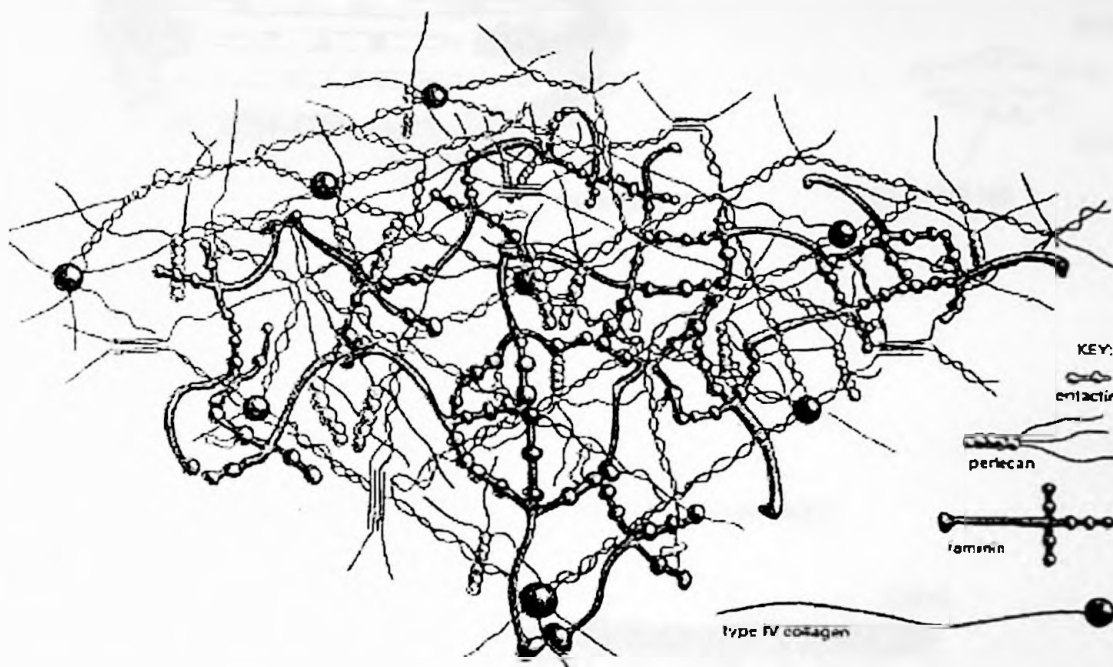
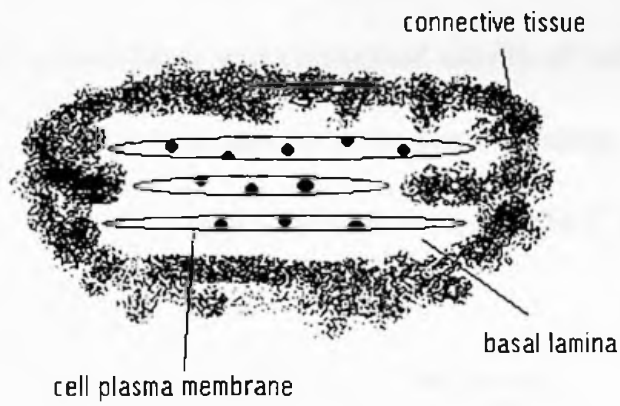


Figure 6. Molecular Structure of Basal Laminin.¹⁵

They underlie all epithelial cell sheets and tubes. They also surround individual muscle cells, fat cells, and Schwann cells. This lining separates the cells from surrounding connective tissue. In other cases, such as with the kidney glomerulus and lung alveolus, the basal lamina is in between two cell sheets, acting as a filter. Basal laminae may also serve to determine polarity, influence cell metabolism, organize the proteins in adjacent plasma membranes, induce cell differentiation and serve as specific highway for cell migration. Figure 7a shows the three different ways basal laminae may be organized.¹⁵

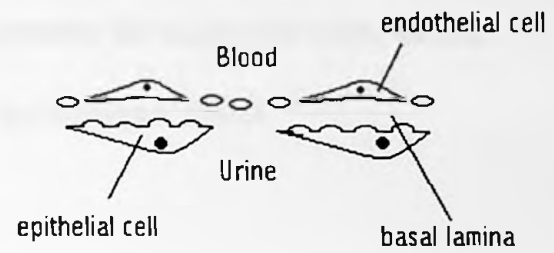
1.

MUSCLE



2.

KIDNEY GLOMERULUS



3.

EPITHELIAL SHEET

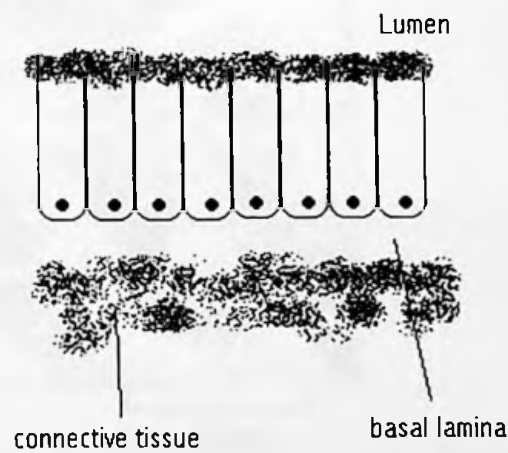


Figure 7a. The Three Different Ways Basal Laminae Organize.¹⁵

Some cell biologists use the term basal lamina and basement membrane interchangeably to describe the three layers of basal lamina. Most basal laminae consist of two distinct layers; an electron lucent layer (lamina lucida or rara) and an electron dense layer (lamina densa). In some cases a third layer was comprised mostly of collagen fibrils (lamina fibroreticularis). Figure 7b is an electron micrograph of the basal laminae. The E represents the epithelial cells, the BL represents the matlike basal lamina, and the C represents the collagen fibrils.¹⁵

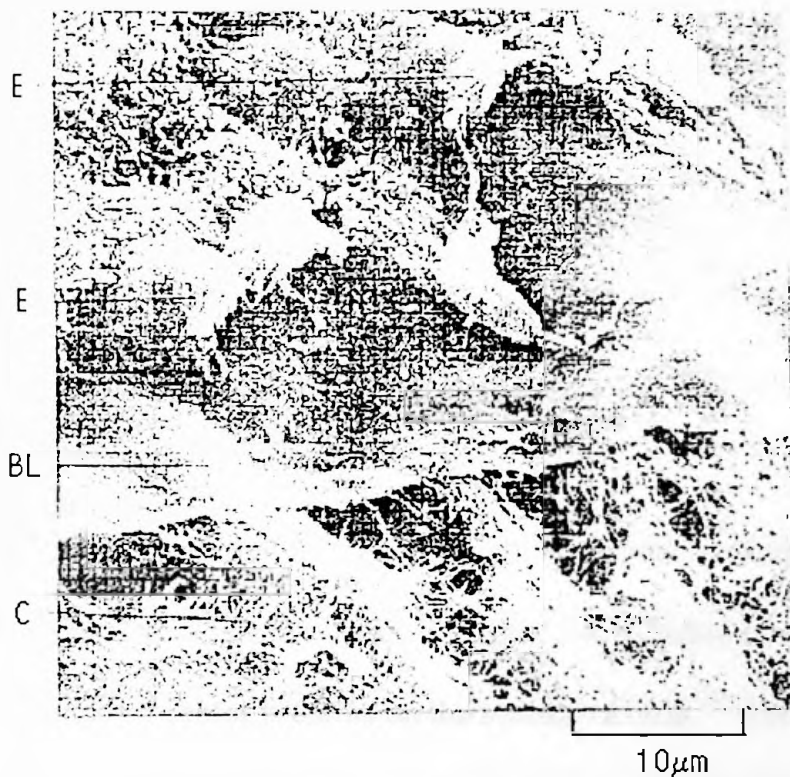


Figure 7b. Electron Micrograph of Basal Laminae.¹⁵ (E) Represents the epithelial cells. (BL) Represents the matlike basal lamina. (C) Represents the collagen fibrils.

Laminin is a large (~850,000 daltons) flexible complex of three long polypeptide chains arranged in the shape of an asymmetric cross and held together by disulfide bonds (Figure 8).^{16,15}

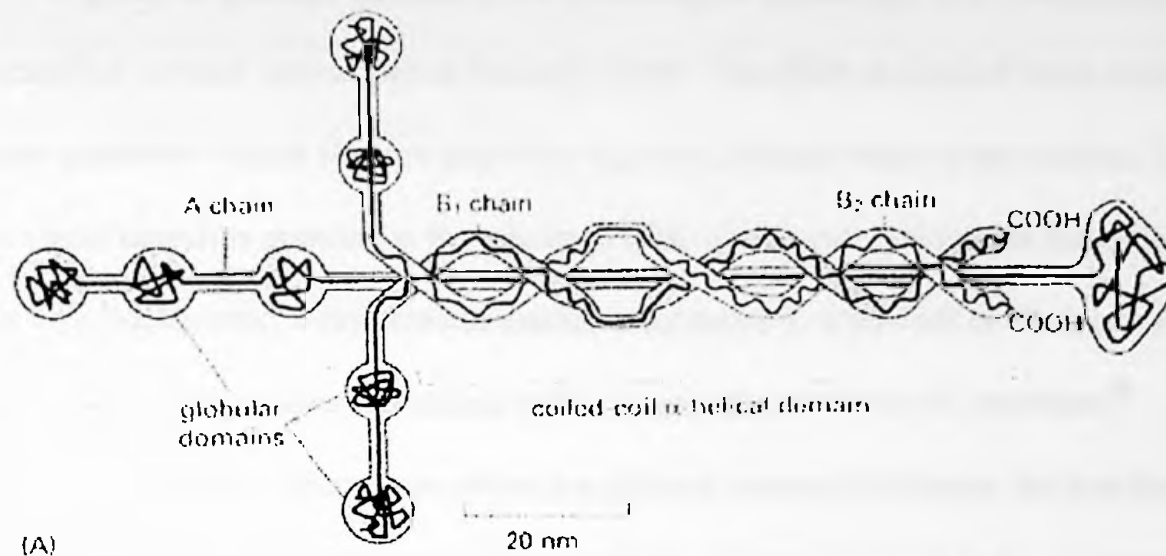


Figure 8. Schematic of Laminin Structure.

Like the other proteins in the extracellular matrix, laminin consists of a number of functional domains: one binds to type IV collagen, one to heparan sulfate, one to entactin, and two or more to laminin receptor proteins on the surface of cells.¹⁷ Laminin is responsible for many kinds of cell basement membrane interactions such as adhesion, migration, or propagation. In cell culture, laminin induces morphologic changes, for example cell spreading, elongation and neurite outgrowth.^{18,19}

Scanning Electron Microscopy (SEM).

A group of graduate students at the University of Cambridge, U.K., originally developed the scanning electron microscope in the early 1950s. The SEM consists of three elements: 1. a vacuum chamber with an electron gun at the top and a sample holder at the bottom; 2. one or more signal detectors pointing at the specimen (The instrument used has the following detectors; secondary, backscatter, x-ray, and cathodoluminescence); 3. a network of electronics to raster a focused electron beam over the sample and to acquire signals from the detectors.²⁰

In any electron microscope, there is a primary source of electrons, the gun (the instrument used has a tungsten filament). When these primary electrons interact with a specimen in a vacuum, they are scattered. These interactions can either be elastic or inelastic.²⁰

Elastic scattering results from the interaction of primary electrons with the electrostatic potentials of the atoms of the specimen. After interacting with the atoms of the specimen about 30% of the primary electrons reemerge from the sample, giving rise to a backscattered electron signal (BE). Inelastic scattering transfers energy from the beam electrons to the atoms of the specimen, decreasing their kinetic energy. Interaction of the primary electrons with the atoms that make up the specimen lead to the transfer of energy (0-50eV) and the ejection of loosely bound electrons from the sample. The low energy ejected electrons, referred to as secondary electrons (SE), and is produced at a shallow sampling depth as a consequence of their low kinetic energy. In addition to the generation of secondary electrons, inelastic scattering also leads to the generations of characteristic x-rays.²⁰

There are many advantages of a SEM instead over a conventional light microscope. The SEM has a large depth of field, which allows a large amount of the sample to be in focus at one time. The SEM also produces images of high resolution, which means that closely spaced

features can be distinguished at high magnifications. Sample preparation is relatively easy since most SEMs only require the sample to be conductive. The combination of higher magnification, larger depth of focus, greater resolution, and ease of sample preparation makes the SEM one of the most heavily used microscope today.²⁰

Confocal Microscopy.

The first stage scanning confocal microscope was made in 1957 by a postdoc at Harvard named Minsky. His microscope was not commercially unfeasible because the technology needed to produce useful images was not available at the time. In 1986-87, a confocal microscope with the capabilities of producing very useful images could be built by combining the technologies of laser, computer, and microelectronics. Amos and White built the first prototype incorporating these technologies and obtained far superior in-focus confocal images of, for example, *C. elegans* embryos.

Figure 9 diagrams the essential features of the confocal microscope.

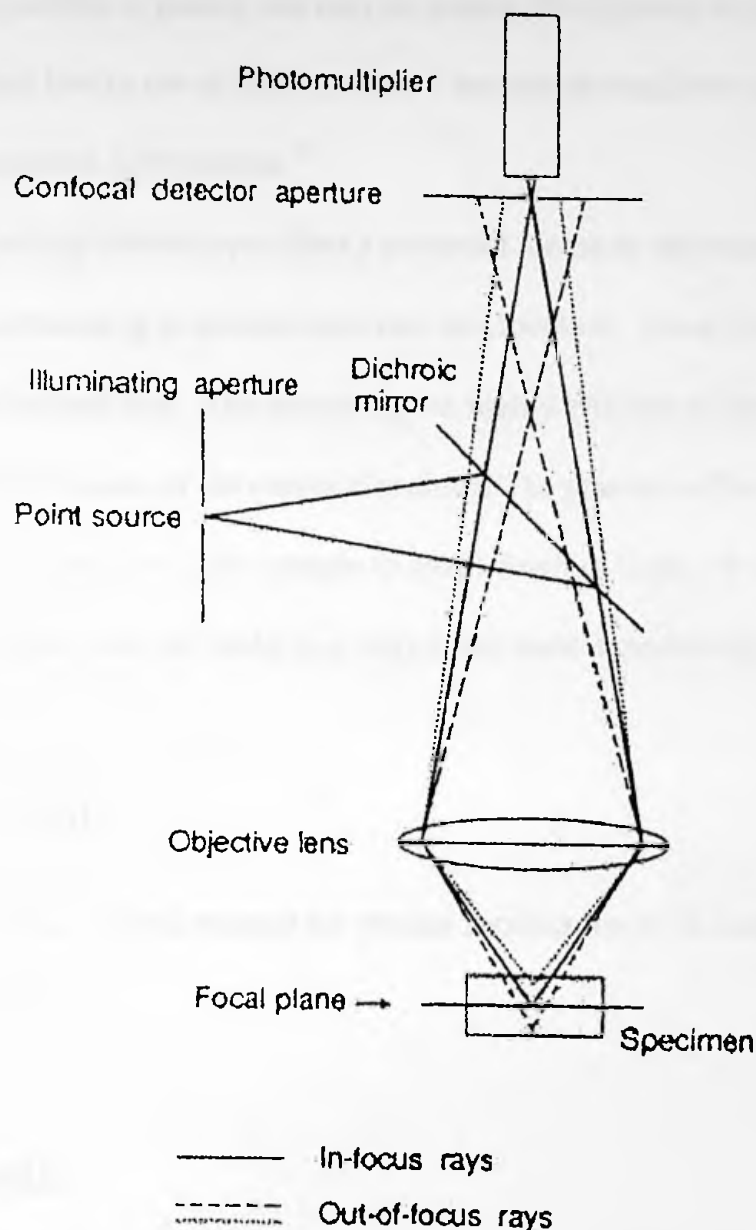


Figure 9. Features of a Confocal Microscope.²¹ A laser source is reflected off the dichromatic mirror toward the specimen. Emitted light from the fluorescence specimen is allowed to pass through the dichromatic mirror toward the photomultiplier detector. The confocal pinhole blocks the out of plane emission light by being conjugate to the laser source pinhole.

A laser is used to provide the source to excite samples, which are themselves luminescent or contain fluorescent dyes. A dichromatic mirror reflects the laser light. This mirror reflects light below a certain wavelength, and passes light above that wavelength. Only the light emitted from

the fluorescent sample is passed and may be seen in the eyepiece or by the detector. The confocal pinhole blocks out of plane emission because the emission pinhole is aligned conjugate to the laser excitation light pinhole.²¹

The confocal microscope offers a powerful means of addressing biological problems and gives new understanding to cellular structure and function. Some advantages of the confocal systems are described here. The microscope is highly efficient at rejecting out of focus fluorescent light because of the confocal pinhole. The practical effect of this is that the image comes from a thin section of the sample (a small depth of field). By scanning many thin sections through the sample, one can build up a very clean three dimensional image of the sample.²¹

Project Goal:

To develop a novel method for protein localization to be used for culturing isolated cells on glass coverslips.

Hypothesis:

In this thesis, the hypothesis for fabricating protein patterns on a coverslip was tested. This hypothesis involves the chemical interaction between hot alcohol and the surface of a glass coverslip, forming a layer of estersil on the surface. Electron bombardment of this film will result in locations with higher protein affinity. An illustration of the method proposed to test this technique is given in Figure 10.

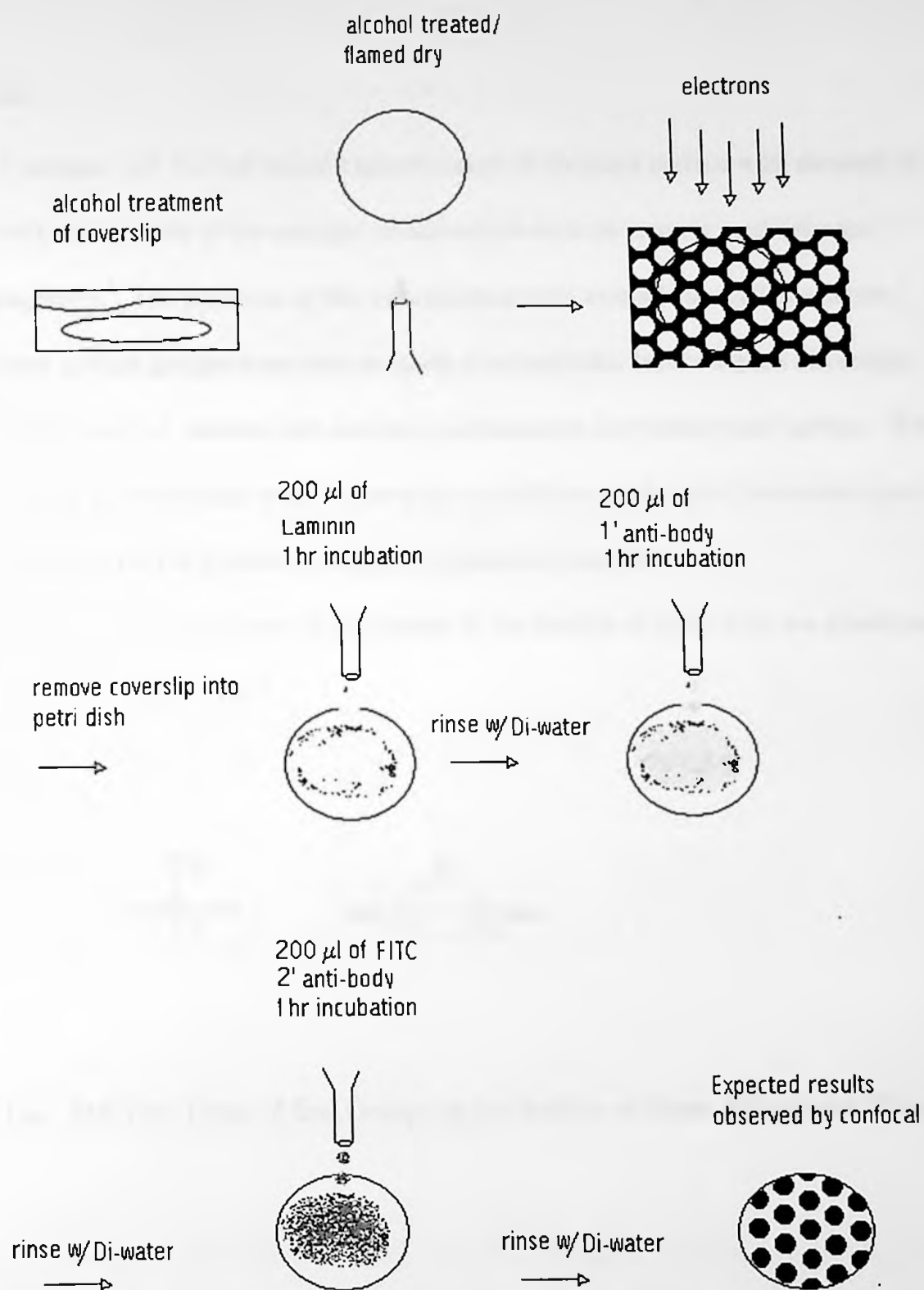


Figure 10. Schematic Diagram of Proposed Process for Producing Protein Patterns.

Estersils:

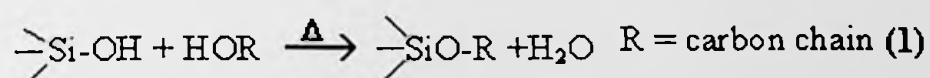
Cadogan, and Sawyer utilized esterification of the silica surface with alcohols in 1970 to reduce the heterogeneity of the energies of adsorption sites on support media for gas chromatography.⁶ The products of this esterification with alcohols are called estersils.⁶ In this thesis, these surface groups were used to create a hydrophobic layer on glass coverslips preventing protein (i.e. laminin and anti-body) adhesion to the treated glass surface. When the treated surface is bombarded with electrons the estersils are replaced by ionizable hydroxyl groups, allowing for the protein to adhere by electronic attraction.

There are only two types of end groups at the surface of glass, they are silanol and siloxane groups (Figure 11a):⁴



Figure 11a. The Two Types of End Groups on the Surface of Glass, Silanol and Siloxane.

When glass (coverslips) are heated with an alcohol (i.e. methanol or ethanol) the reaction is as follow (1):



The surface of glass is slightly acidic (isoelectric point of silica has a pH of 2). The silanol being slightly acidic and the siloxane acting like an acidic anhydride reacts with the alcohol forming the hydrophobic layer of estersils.²¹ Figure 11b illustrates the silanol mechanism with methanol.

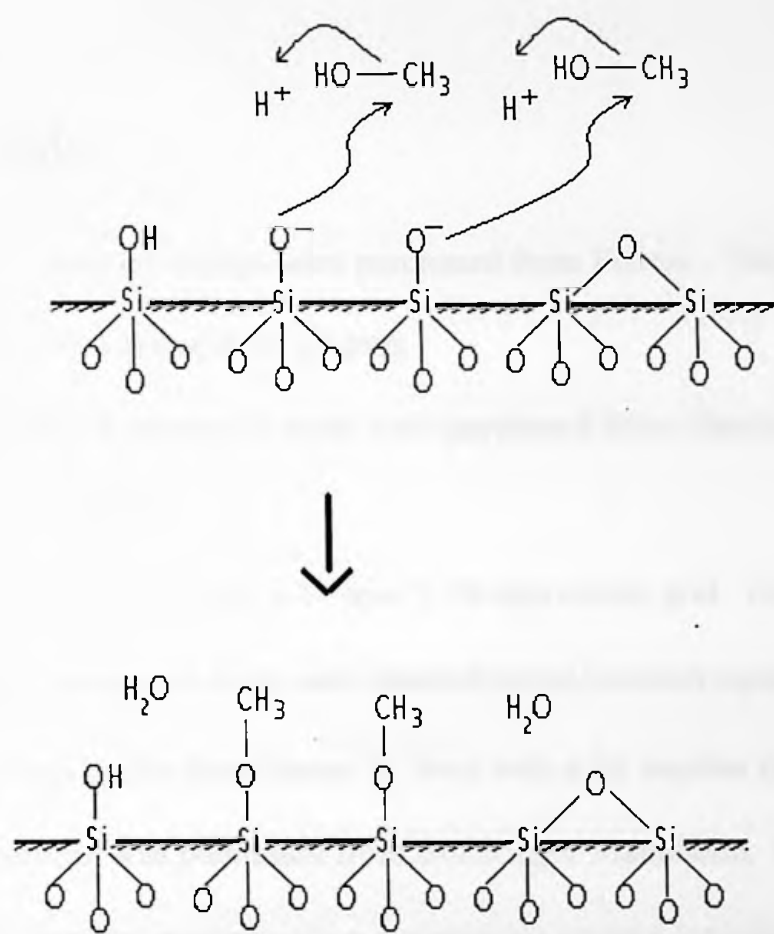


Figure 11b. Methanol Reacting with Glass Surface.

Electron irradiation will break up the SiO-R bond resulting in Si-O⁻, which can easily be protonated with hydrogen from water in the air or vacuum chamber. The patterned surfaces were treated with fluorescent antibodies and observed using the confocal fluorescence microscope.

Instrumentation:

The scanning electron microscope (SEM) used was a JEOL JSM-5310LV.

The confocal microscope used was a Bio-Rad MRC-1024.

Materials:

The glass coverslips were purchased from Fischer. They are standard circular microscope coverslips with a diameter of 18-mm.

The SEM aluminum stubs were purchased from Electron Microscopy Sciences, having a diameter of 35-mm.

The mask used was a 24-mm X 19-mm nickel grid. Circular holes (with a diameter of 90- μ m) in a hexagonal array were electroformed (etched) equally from both sides. The grids were supplied by Buckbee-Mears St. Paul with a lot number of 2-1-8.

Laminin was purchased from Boehringer Mannheim. Its original concentration was 500- μ g/ml. To prevent contamination and prolong protein activities, the protein was separated into 20 different vials and kept in a -20.0⁰C freezer. Once a vial was thawed and used it was kept refrigerated but not frozen due to the adverse effect of continual freezing and thawing.

The primary anti-body (rabbit polyclonal to laminin) was purchased from Polyscience Incorporated.

The secondary fluorescein isothiocyanate (FITC) antibody and the natural goat serum (NGS) were purchased from SIGMA.

Experimental: Standard Methods

Flame Drying:

A glass coverslip was immersed in an alcohol and removed with a clean tweezer, then quickly touched to the flame of a Bunsen burner. The alcohol was allowed to burn completely off the coverslip. Treated glass coverslips were found to be hydrophobic upon applying water droplets on its surface.

Dichlorodimethylsilane Treatment:

A coverslip removed from a methanol bath was allowed to air dry. Once dried, four drops of dichlorodimethylsilane were pipetted (with a 1-ml pipette) into the petri dish away from the coverslip and then the lid was replaced until the dichlorodimethylsilane completely evaporated (~ 30min). The coverslip was removed for further experiments.

Laminin Treatment:

A 200- μ l drop of laminin was pipetted (200 μ l micropipette) and allowed to incubate at room temperature for 1-hr. After the 1-hr incubation, non-binding laminin was rinsed off with

deionized water. Laminin was diluted from its original concentration (500- μ g/ml) to the working dilution of 10- μ g/ml. A milliliter of laminin was made by pipetting 20- μ l from the original concentration and diluted to 1-ml with phosphate buffered saline (PBS) (pH of 7.4). The coverslip was incubated in a closed petri dish.

Primary Antibody Treatment:

A 200- μ l drop of primary rabbit antibody polyclonal to laminin was pipetted and allowed to incubate for one hour. Again after incubation, non-binding antibodies were removed using deionized water. One milliliter of the primary antibody was prepared by adding 1- μ l of the antibody in 5% NGS (50- μ l) and diluted to 1-ml with PBS. The coverslip was incubated in a closed petri dish.

Secondary Antibody (FITC) Treatment:

A 200- μ l drop of the secondary anti-rabbit fluorescein isothiocyanate (FITC) conjugated antibody was pipetted onto the coverslip and allowed to incubate at room temperature for 1-hr in a dark area. A thorough rinse with deionized water was necessary to remove non-binding antibodies. The secondary antibody (FITC) was prepared by adding 6.25- μ l of the antibody in 5% NGS and diluted to 1-ml with PBS. The coverslip was incubated in a closed petri dish.

Mounting and Removing Coverslip:

Coverslips were mounted on the SEM's aluminum stub with an adhesive paint. A thin layer of the adhesive paint was applied to the stub, which allowed easy removal of the coverslip. Double-sided carbon tape was not used because the coverslip could not be removed without breaking, due to its stronger adhesion to the coverslip. The nickel grid was also held in place by adhesive paint at an edge of the coverslip. The stub was then secured onto its holder and placed into the SEM's vacuum chamber.

The nickel grid was carefully removed with a tweezer so that the grid did not warp. Then the coverslip was detached from the stub by applying gentle pressure on all sides of the coverslip to slide it off the dry paint. The coverslip was then placed in a petri dish for further experiments.

Standard SEM Parameters: Masked Exposure

Several areas (4 areas near the center of the coverslip) were irradiated with electrons at the following parameters: time of exposure = 30 min., acceleration voltages = 30kV, magnification = X35, spot size 24, working distance (wd) = 20, and load current = 98 μ A.

Preparation of Coverslip for Observation under the Confocal:

After all the needed protein treatments the coverslip was adhered to a microscope slide with the treated side facing up, using epoxy. The prepared slide was immediately transported to the confocal in a dark closed box for observations.

Standard Confocal Parameters:

All fluorescent patterns were captured using the confocal with the following starting parameters: averaging = Kalman (2 times), magnification = 10X, wavelength = 488nm, laser power = 100%, iris = 8.0, gain = 1500, B-level = 0, and the low sig. button checked for all Mixers (Mixer A, B, and C).

Quantitation of Intensities:

Ten pixel wide line intensity scan across four patterns were quantitated using Bio Rad's proprietary laser sharp software. The raw data points were plotted with excel. The line intensity graphs were smoothed using a 10-point moving average. The intensity scale is 0-256 in arbitrary units of intensity. The tabulated averages were calculated using the raw data at the specified intervals.

Experiments: Results and Discussions

The following experiments may be categorized into two types, those involving the use of a nickel mask and those performed by using a electron beam direct write method.

SEM micrographs were taken of the nickel grid in order to be sure that there is not any imperfection (i.e. ridges around the holes) on the grid that may be a factor in the following experiments. As expected there were no apparent ridges that may scratch the surface of the glass coverslips used in these experiments (Figures 12a and 12b).

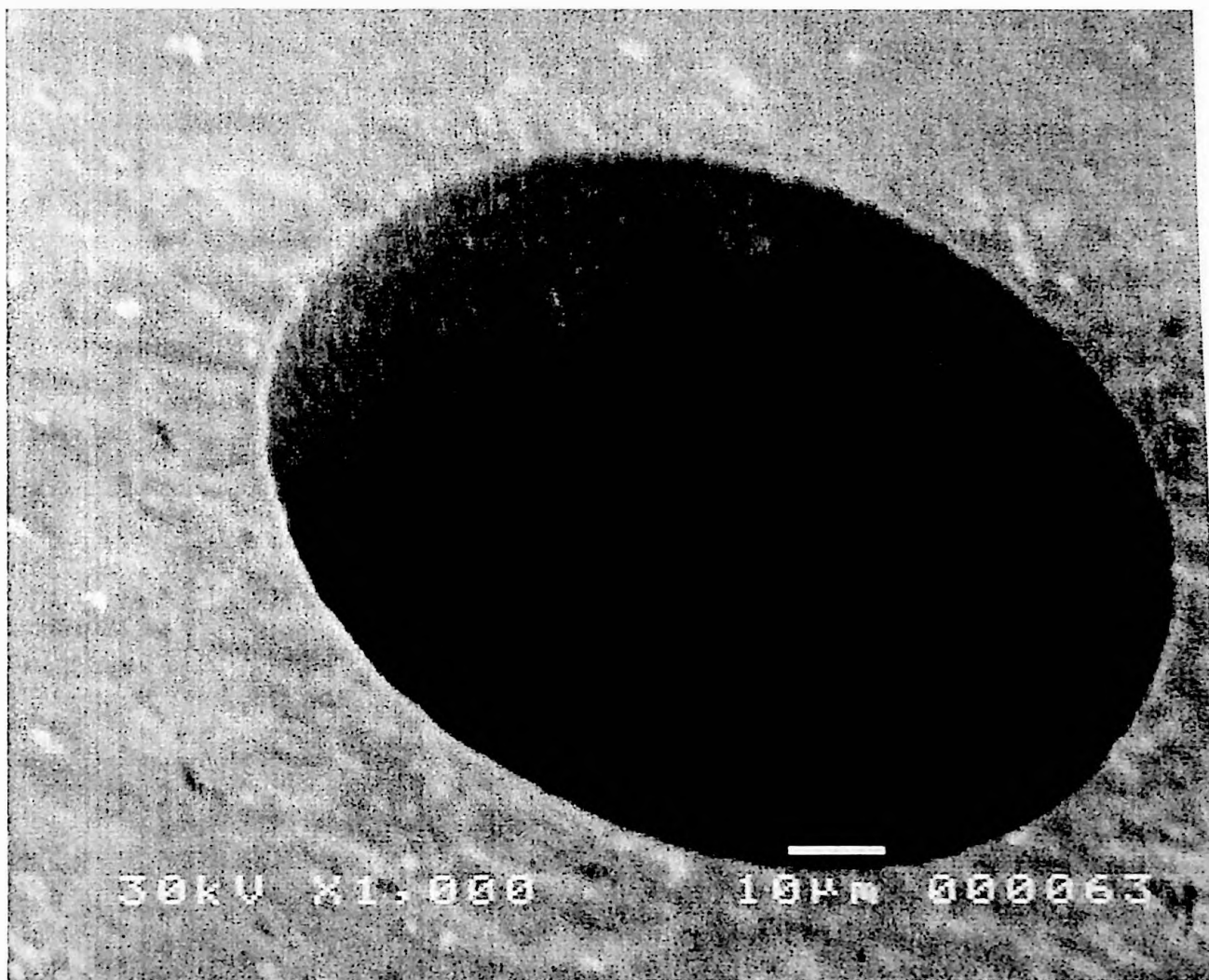


Figure 12a. SEM Micrograph of the Nickel Grid. This micrograph was taken to find an abnormality at the edge of the circular holes that might interfere with the experiments. There were no such abnormality found.

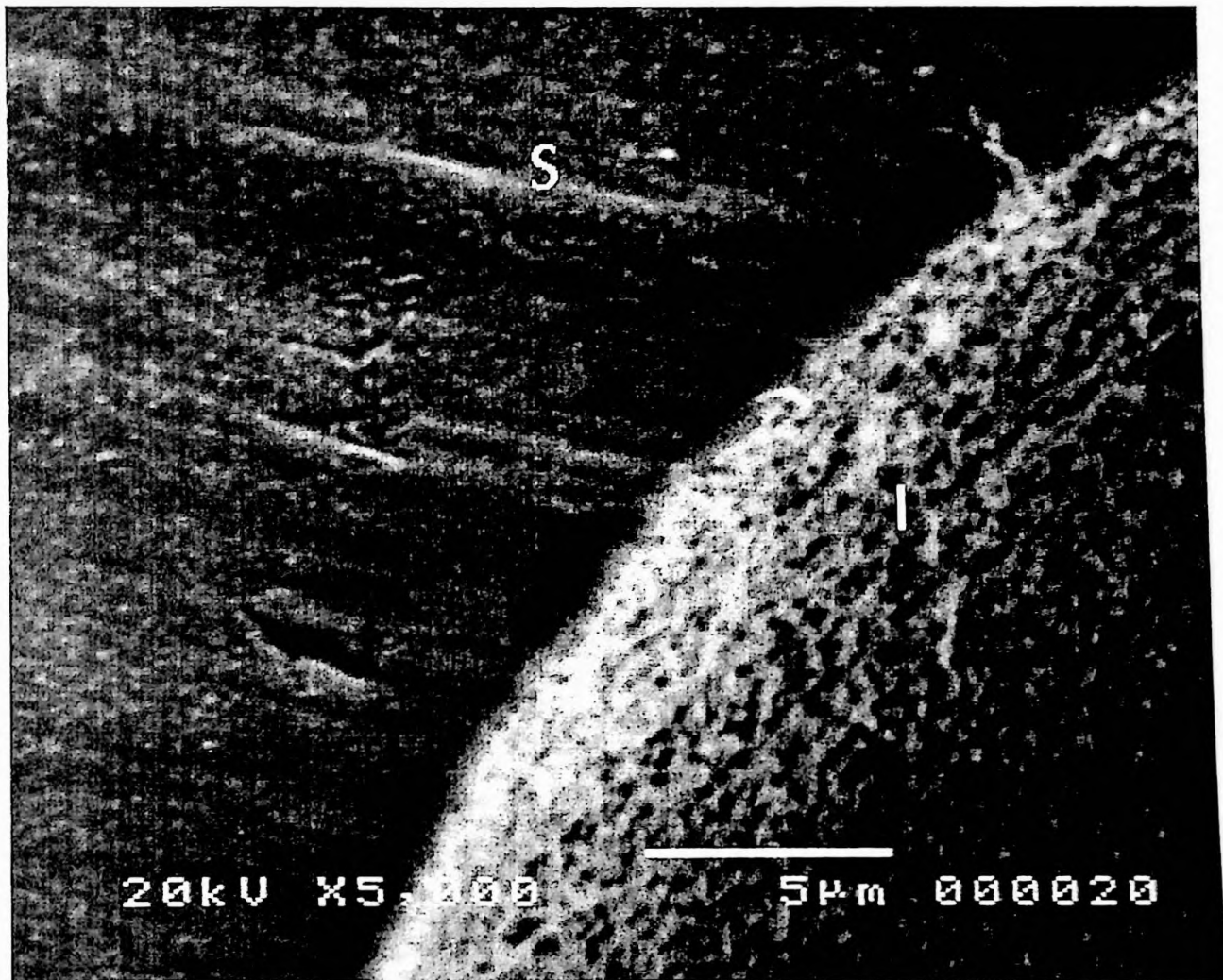


Figure 12b. SEM Micrograph at the Edge of the Circular Hole of the Nickel Grid.
(S = top surface, I = inside of hole)

Nickel Mask Experiments:

Dichlorodimethylsilane Treatment before Electron Irradiation (Sample A):

This experiment was performed to prove that the presence of a methyl layer reduces the affinity to protein. A coverslip was treated with dichlorodimethylsilane. After the treatment, the coverslip was masked, placed in the SEM and irradiated at the standard SEM parameters in two areas. After the irradiation, the coverslip was removed from the SEM and treated with laminin, primary antibody and secondary antibody. Patterns were captured using the confocal at the standard confocal parameters.

A possible reaction between the dichlorodimethylsilane and the glass surface is (2):

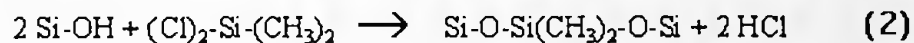


Figure 13 diagrams the mechanism for this reaction.

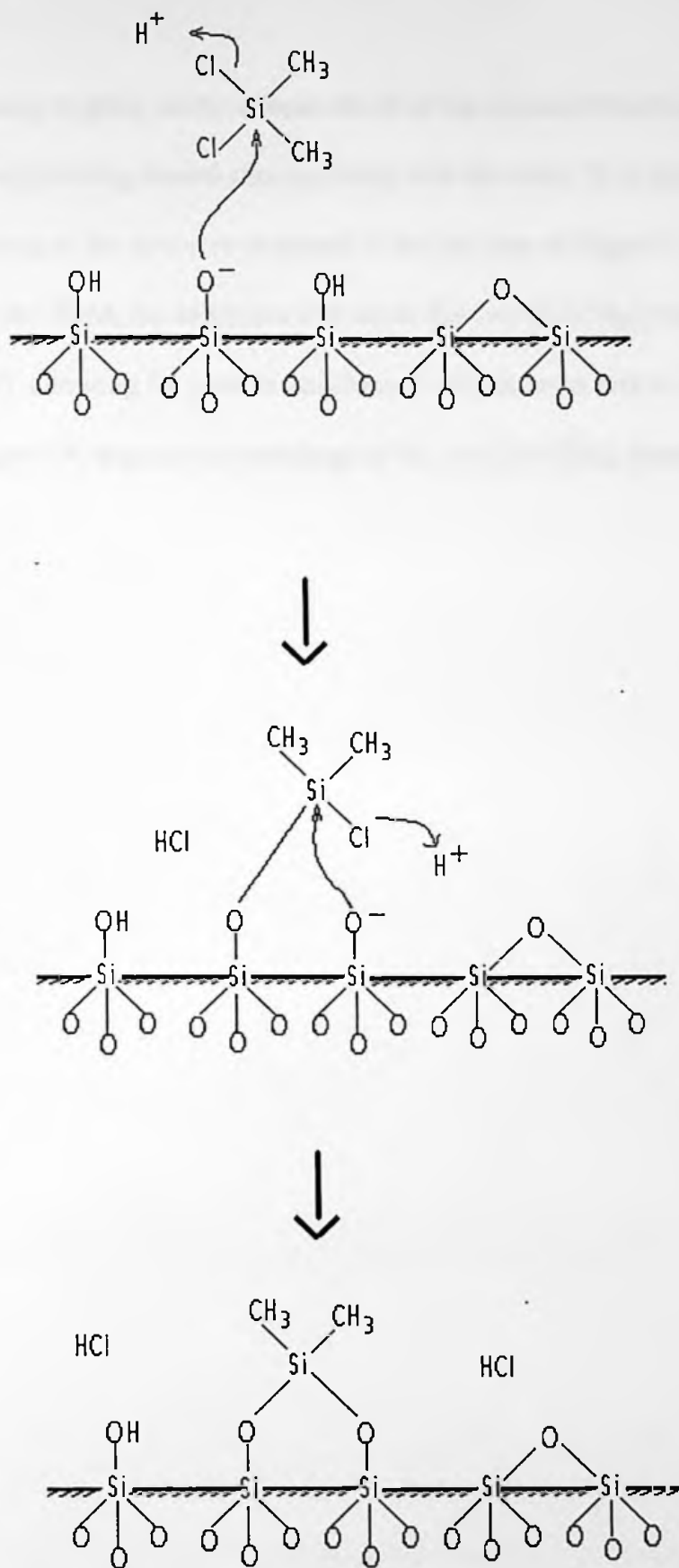


Figure 13. Reaction of Dichlorodimethylsilane with the Surface of Glass.

The silanol, being slightly acidic attacks the Si of the dichlorodimethylsilane displacing the chlorine. A neighboring silanol also can react with the same Si to displace the remaining chlorine resulting in the structure depicted in the last step of Figure 13.

Under the SEM, the electrons will break the two Si-(CH₃)₂ bonds returning the glass surface to Si-O⁻ allowing for protein attachment only in areas where electron bombardment occurred. Figure 14, depicts this breakage of the two Si-(CH₃)₂ bonds and the adhesion of protein.

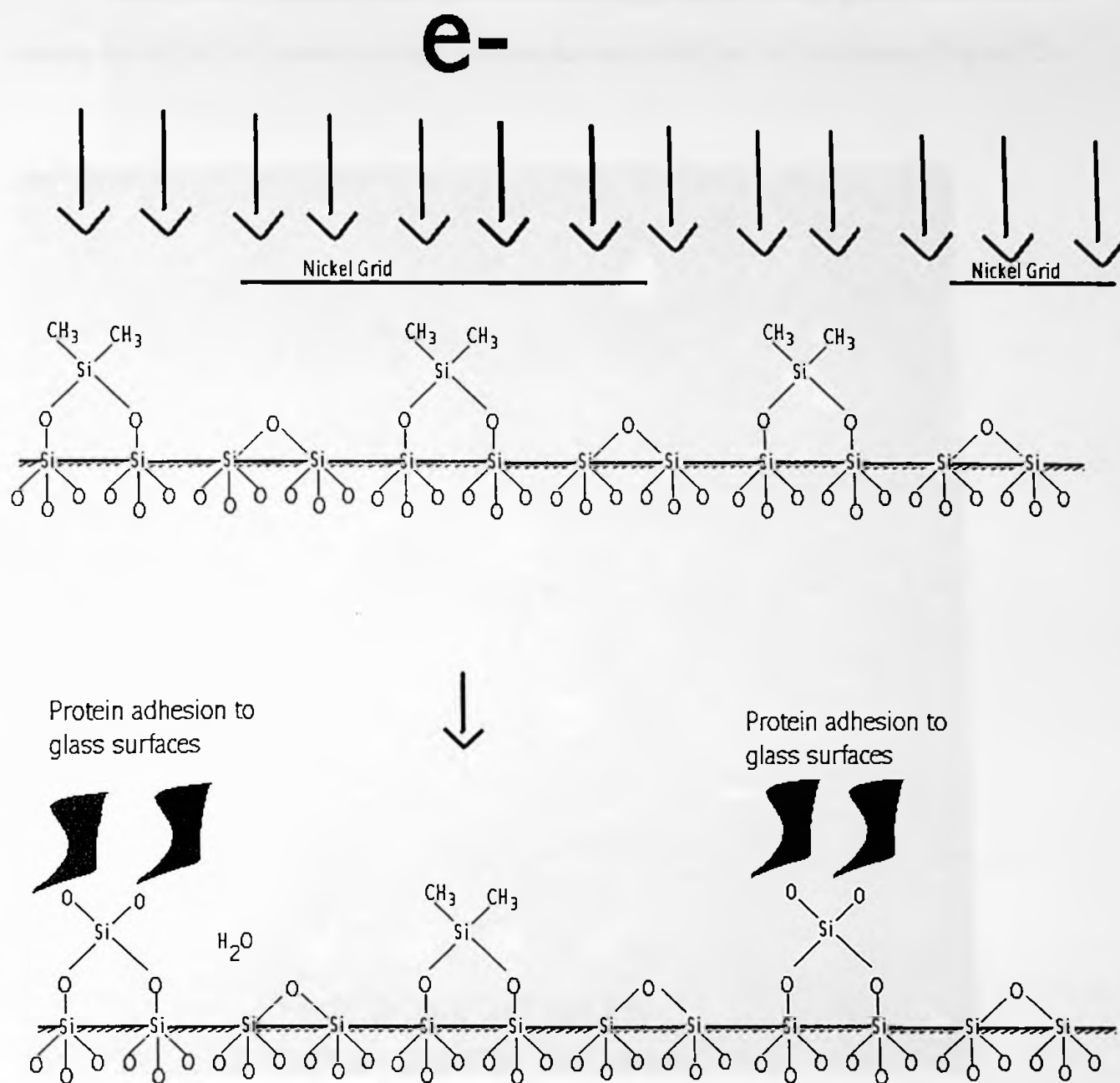


Figure 14. Bond Breaking Due to Electron Bombardment, Allowing for Protein Adhesion.

The average bond energy for Si-C is 72 kcal/mol and for Si-O is 108 kcal/mol,²¹ therefore, the Si-CH₃ bonds are more likely to be broken than the (CH₃)₂Si-OSi bonds.

As expected, patterns were observed indicating that the methyl group does seem to reduce the affinity of protein, except in areas that are irradiated with electrons (Figure 15).

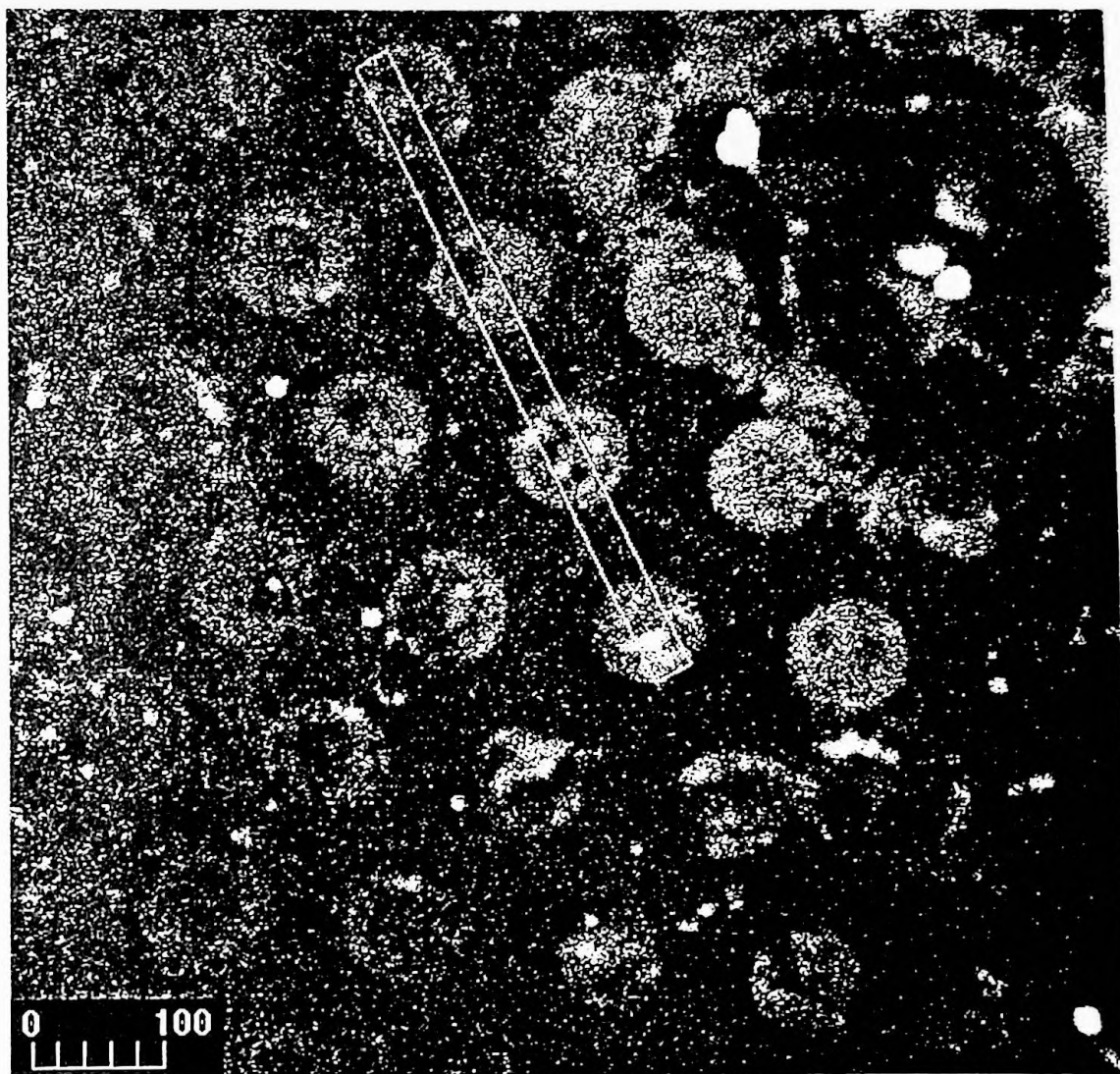


Figure 15. Confocal Micrograph of Sample A. The rectangular drawing represents the 10-pixel wide line intensity measurement. Confocal parameters: averaging = Kalman (2 times), magnification = 10X, wavelength = 488nm, laser power = 100%, iris = 8.0, gain = 1500, B-level = 0, and the low sig. button checked for Mixer A.

Line intensity across four patterns was measured and graphed as shown in Figure 16. The bolder line on the graph represents the 10-point trendline, which helps reduce the noise of the plot so that the patterns and dips are easier to observe.

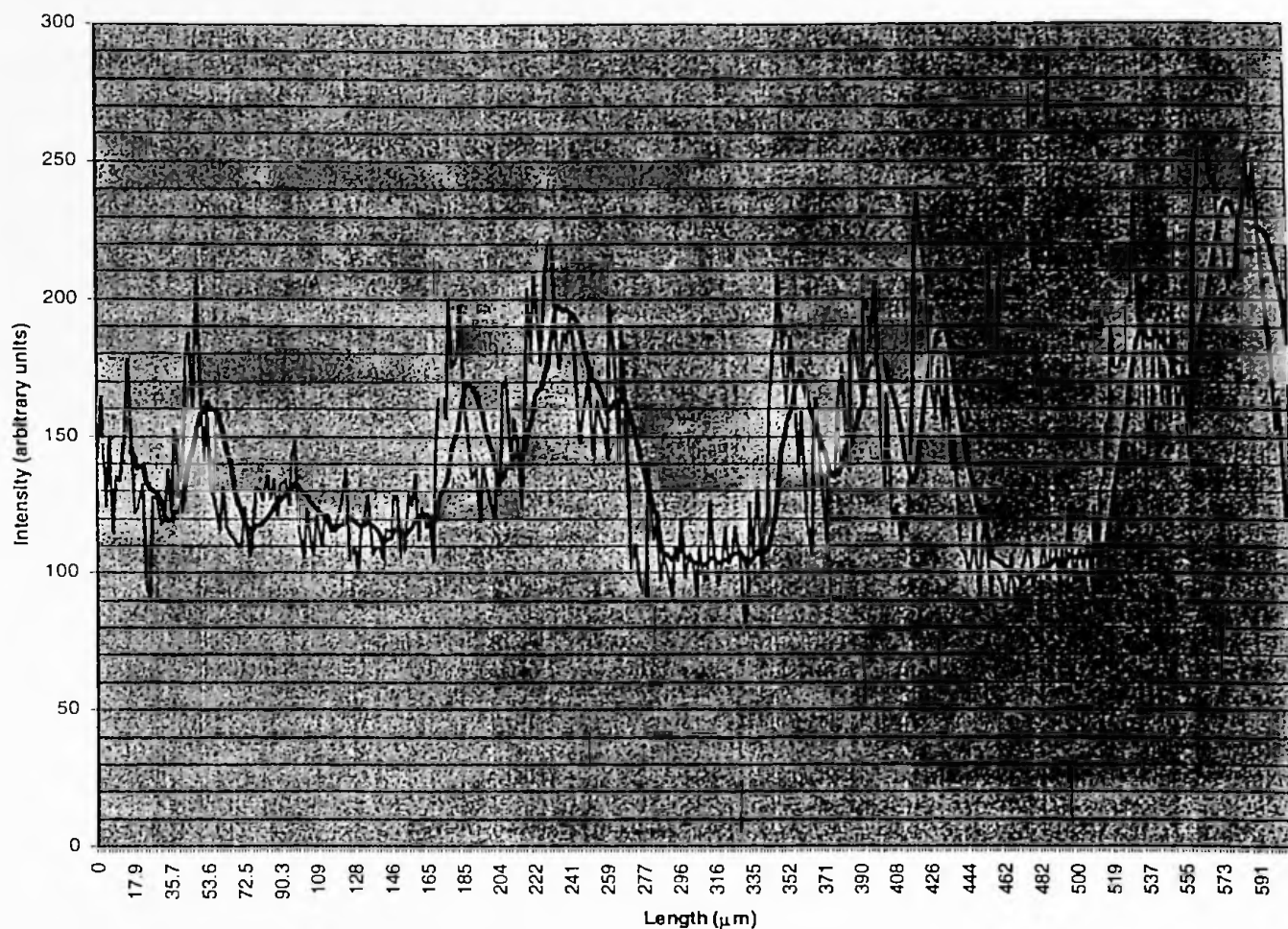


Figure 16. Line Intensity of Sample A. (Light line = raw data) (Dark line = 10 point moving average)

The graph clearly shows the area where the four patterns were made and the differences in intensity when compared to the background. The average intensity of selected areas was calculated and listed in Table 2. There are noticeable differences between the average intensities of the patterns and the background. The signal to background ratio is calculated to be $164.637 / 109.004$ or 1.5.

Table 2. Average Intensities for Sample A

	Avg. Intensity	Length Interval
First pattern	133.792	4.049-98.437
Second pattern	165.792	172.871-269.224
Third pattern	159.165	350.772-441.112
Fourth pattern	199.798	522.661-604.616
Average	164.637	
First background	116.927	101.791-168.822
Second background	106.489	278.998-339.321
Third background	103.595	446.143-512.886
Average	109.004	

Due to the fact that protein adheres to the areas where electron irradiation occurred, one can see that the methyl group may be involved in this patterning technique.

Electron Irradiation after Protein Treatment (Sample B):

This experiment was performed to see if irradiated laminin will be inactivated and shielded laminin remains active. A coverslip was treated with laminin. After the treatment the coverslip was mounted onto an SEM stub. At the standard SEM parameters, the masked coverslip was then irradiated with electrons in two different areas.

After the irradiation process, the coverslip was placed in a petri dish and treated with the primary antibody. Then the coverslip was treated with the secondary antibody (FITC). Finally, the coverslip was observed with the confocal microscope.

As expected, the protein in areas that were irradiated with electrons were inactivated, therefore they appeared darker (less binding with antibodies) (Figure 17).

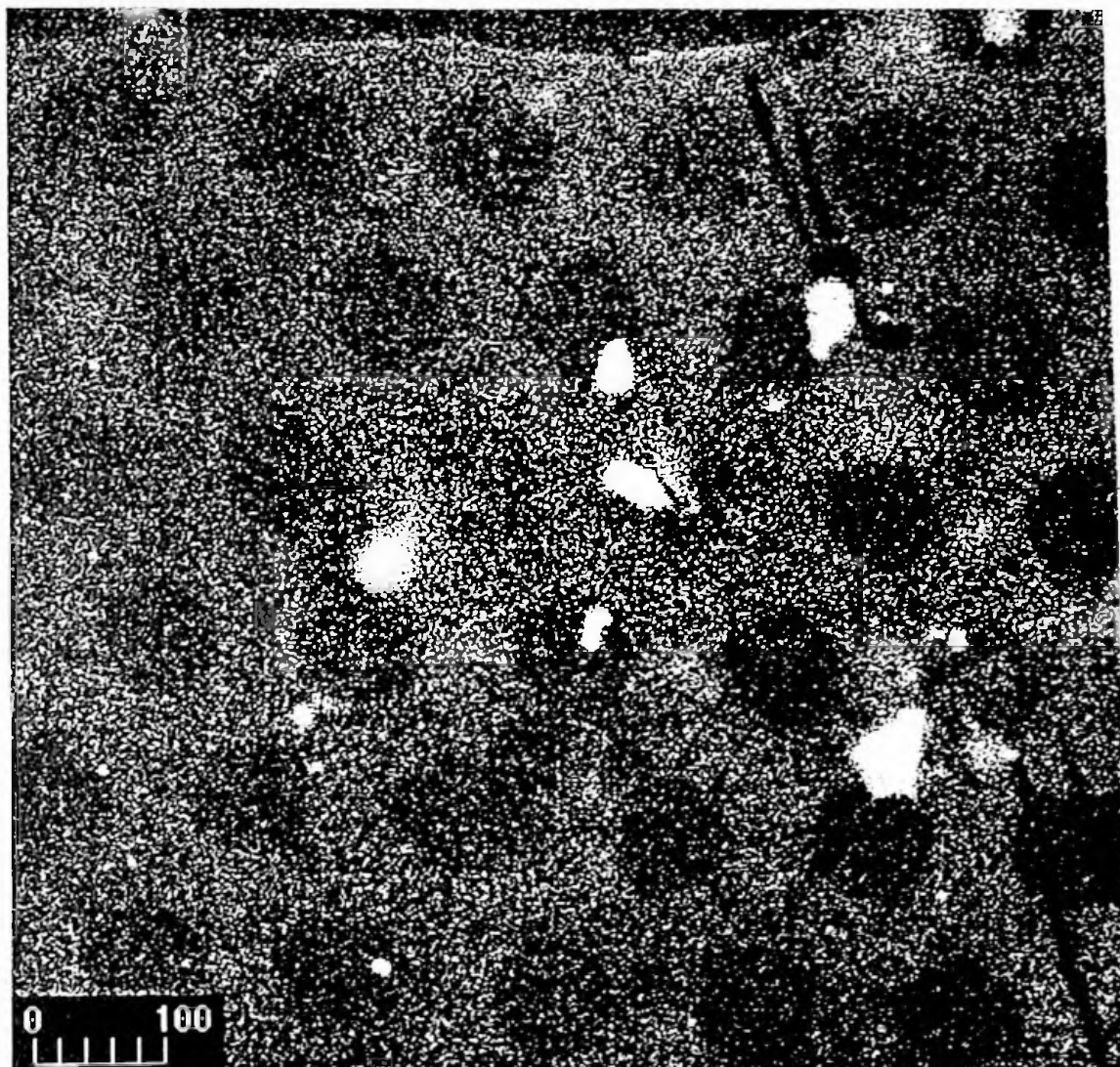


Figure 17. Confocal Micrograph of Sample B. Confocal parameters: averaging = Kalman (2 times), magnification = 10X, wavelength = 488nm, laser power = 100%, iris = 8.0, gain = 1500, B-level = 0, and the low sig. button checked for Mixer A.

The laminin that was shielded from the electrons (under the grid) fluoresced due to its binding with labeled antibody. Line intensities across four of the irradiated spots were determined (Figure 17). Figure 18, is the graph of that line intensity measurement.

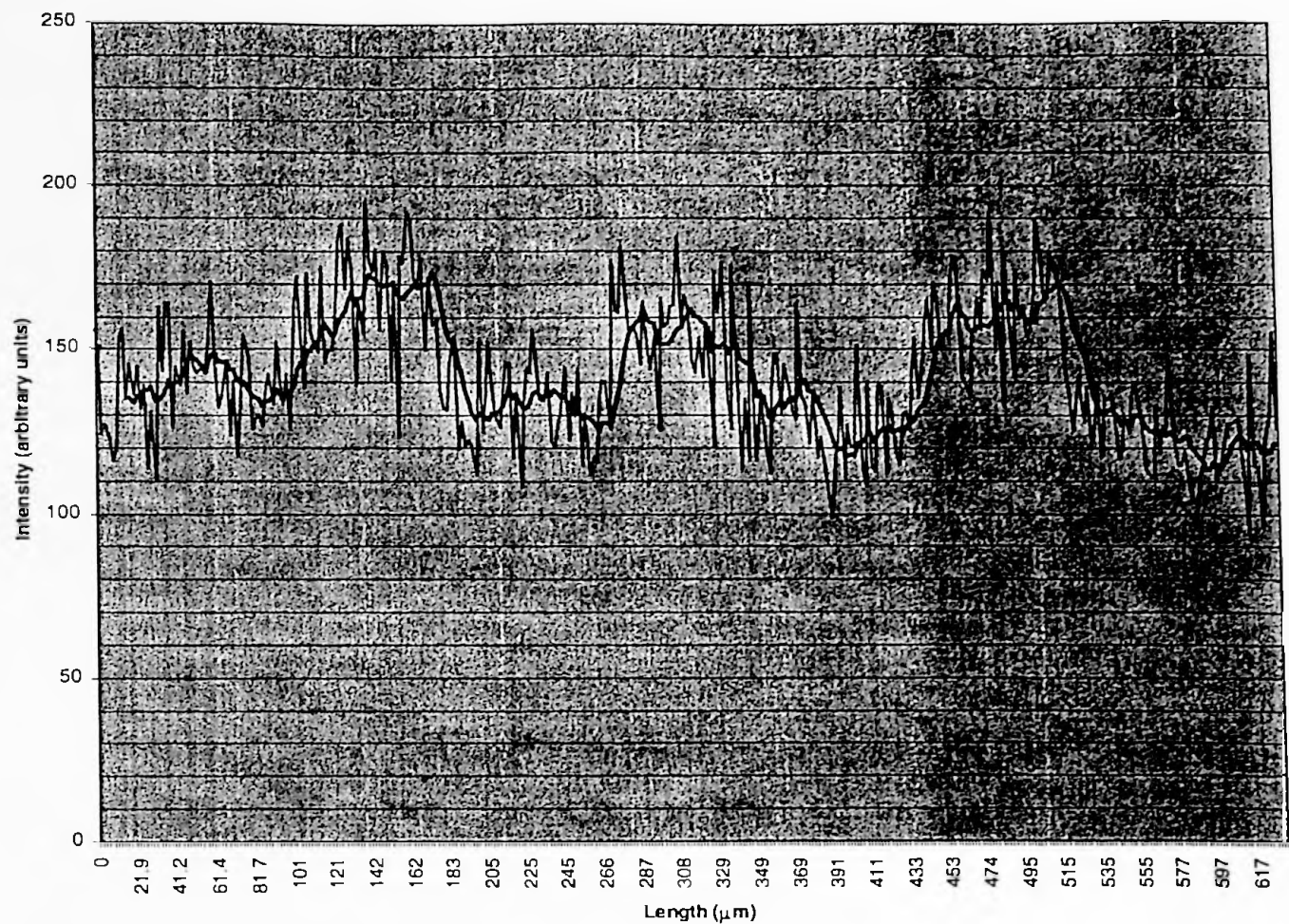


Figure 18. Line Intensity of Sample B. (Light line = raw data) (Dark line = 10 point moving average)

One can see that the four irradiated areas are much lower in intensity (the dips in graph). The three areas of high intensity on the graph represent the intensity of the unirradiated protein. Also, their maximum intensity is relatively consistent.

Table 3 lists the average intensities at certain intervals in the line intensity graph. The average intensity between the protected backgrounds and the irradiated areas is definitely different. The signal to background ratio is $129.521 / 158.727$ or 1.2.

Table 3. Average Intensities of Sample B

	Avg. Intensity	Length Interval
First irradiated spot	139.599	8.09727-98.556
Second irradiated spot	131.869	182.59-264.55
Third irradiated spot	123.091	381.26-435.57
Fourth irradiated spot	123.527	524.933-614.41
Average	129.521	
First background	166.115	103.3-173.51
Second background	149.112	274.32-375.54
Third background	160.953	439.62-515.159
Average	158.727	

Visually from Figure 17 and 18, the intensity of the protected areas is higher than the intensity of the irradiated area. This difference is also visible from the calculation of the average intensity in the selected regions (Table 3). This demonstrates that the irradiated laminin loses its ability to bind with the antibodies while the protected laminin retains its ability to bind to the antibodies, therefore it fluoresces. This experiment was successful. However, the inverse pattern is actually required. This led to the exploration of a method involving estersils.

Electron Irradiation before Protein Treatment (Methanol Flame Dried) (Sample C):

This experiment was performed to test the hypothesis that the formation of estersils reduces the affinity to protein and upon electron irradiation of this layer a hydrophilic hydroxyl layer is exposed for protein adhesion. A coverslip was flame dried with methanol. The coverslip was mounted onto the SEM stub. The irradiation process was directed at two areas near the center of the masked coverslip using standard SEM parameters. Then the coverslip was treated with laminin, primary antibody and then secondary antibody (FITC). Patterns were observed using the confocal at the standard confocal parameters.

In this experiment, flame-drying results in an interaction between methanol and the surface of the glass coverslip, presumably resulting in a layer of estersil (Si-OCH_3). This reaction is depicted in Figure 11. After creating the estersil layer, the coverslip is covered with the nickel grid and placed under the SEM for irradiation. Areas that are exposed to the electron irradiation will result in the breakage of the SiO-CH_3 bond. Once the irradiated coverslip was removed from the SEM and treated with the protein, exposed SiO^- will have more affinity to protein than the SiO-CH_3 (Figure 19).

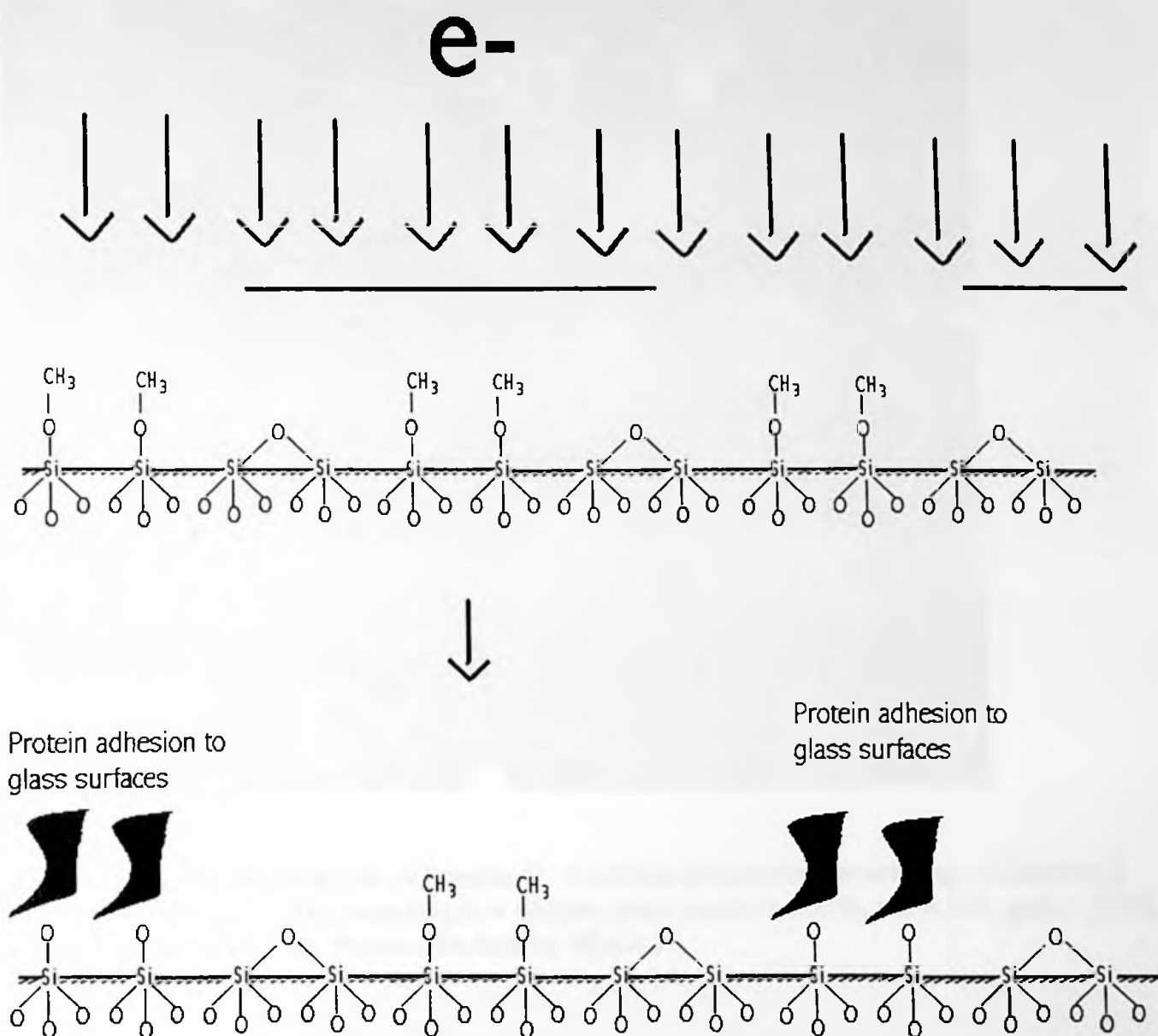


Figure 19. Exposed SiO-CH₃ Bonds are Broken.

Under the confocal, hexagonal arrays were observed, therefore, the hypothesized reaction seems to be occurring. Figure 20 was captured under standard confocal parameters.

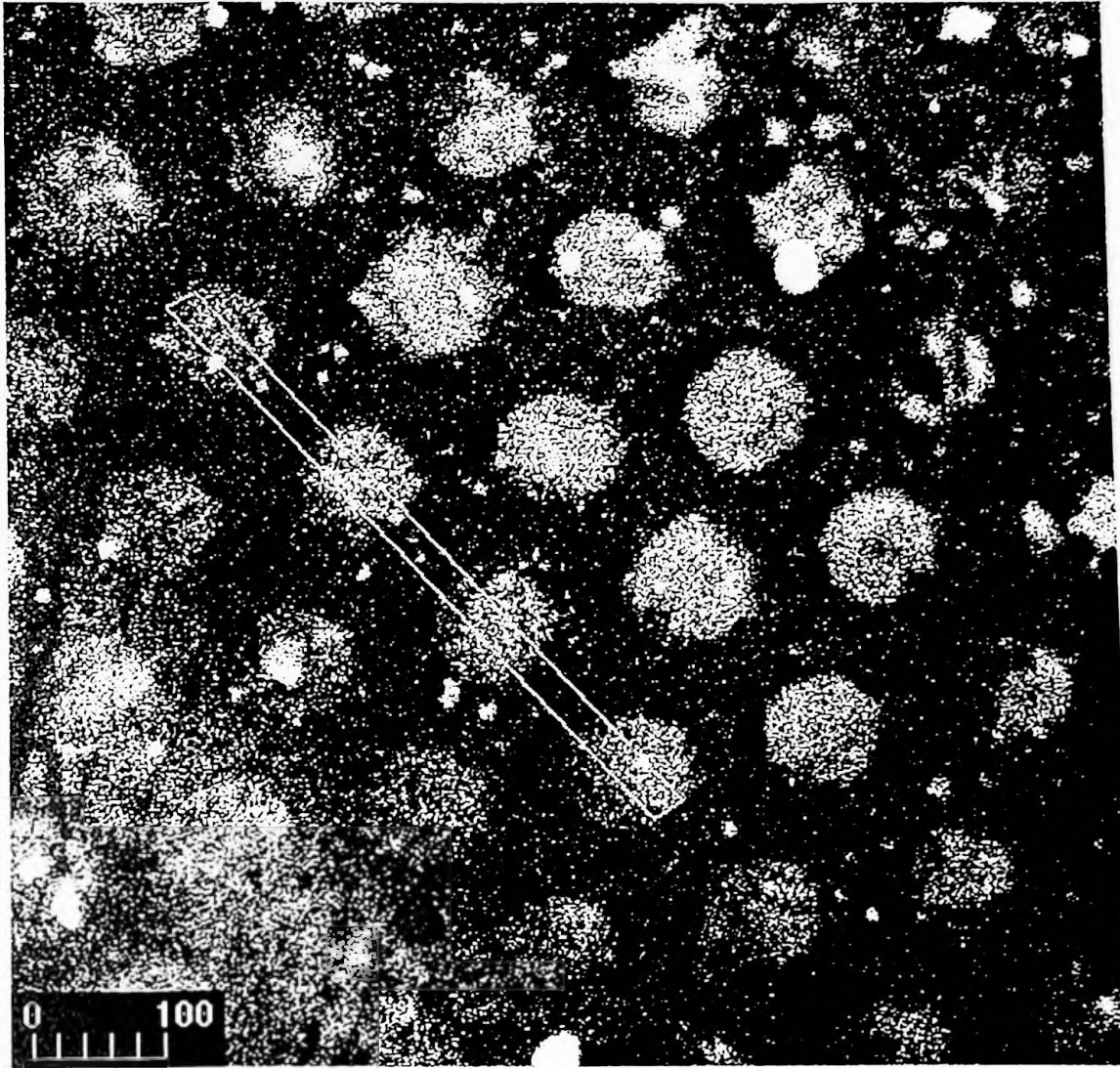


Figure 20. Confocal Micrograph of Sample C. Confocal parameters: averaging = Kalman (2 times), magnification = 10X, wavelength = 488nm, laser power = 100%, iris = 8.0, gain = 1500, B-level = 0, and the low sig. button checked for Mixer A.

Line intensity measurement across four patterns was taken from Figure 20 and graphically depicted in Figure 21.

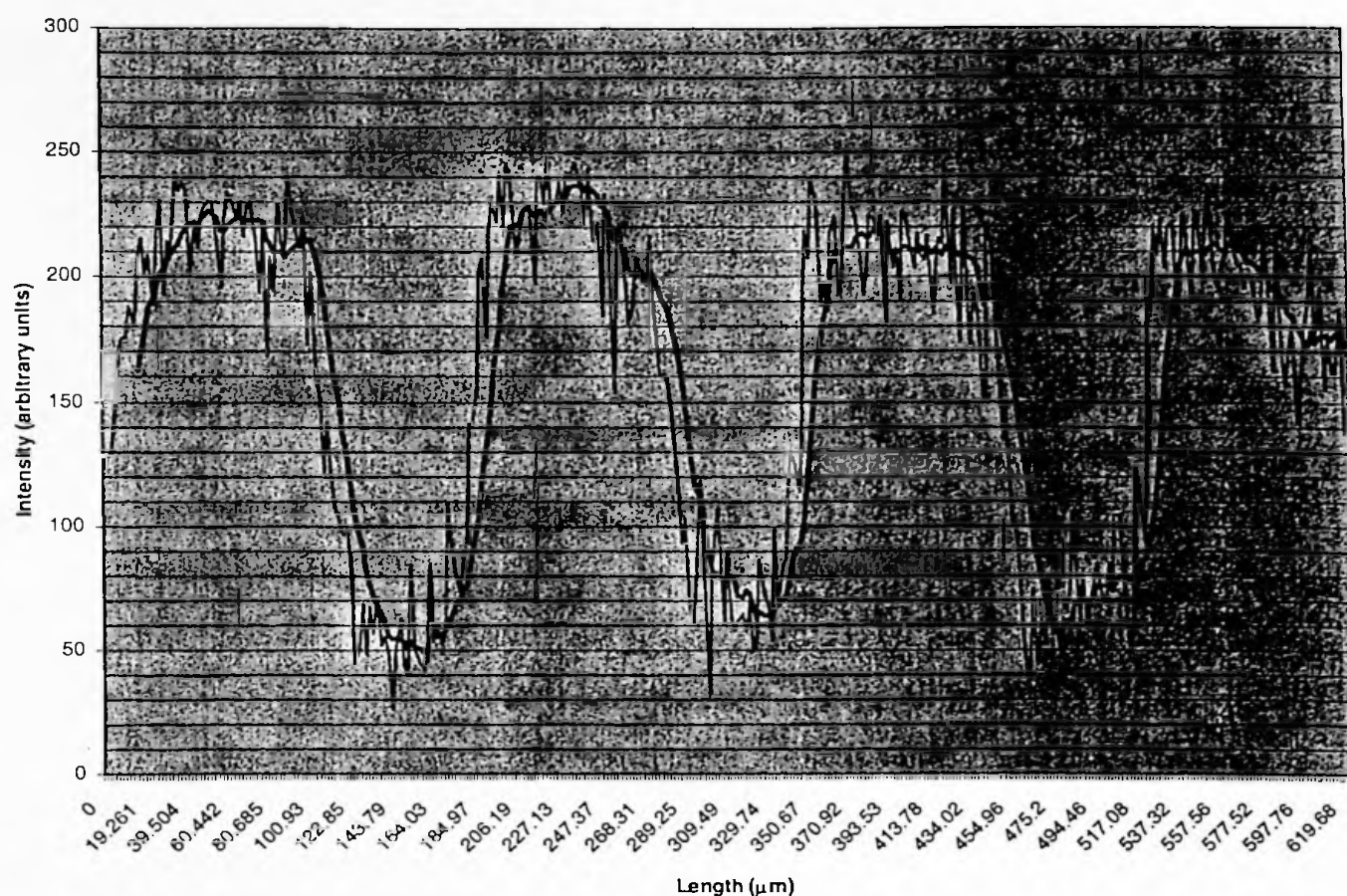


Figure 21. Line Intensity of Sample C. (Light line = raw data) (Dark line = 10 point moving average)

The average intensities of four patterns on this experiment are reported in Table 4 as well as the average intensities of the background. Figure 21, graphically shows the patterns are more intense than the background and according to Table 4, the patterns are approximately three times more intense. The signal to background ratio was calculated to be 3.1. This intensity comparison proves the higher affinity of protein for the areas bombarded with electrons. Therefore, this supports the contention that estersils were involved in blocking the protein from adhesion.

Table 4. Average Intensity of Sample C

	Avg. Intensity	Length Interval
First pattern	216.359	16.8892-100.928
Second pattern	219.688	188.321-274.037
Third pattern	208.722	352.351-446.858
Fourth pattern	195.911	529.22-619.68
Average	210.170	
First background	59.138	122.848-174.498
Second background	71.681	292.603-334.479
Third background	73.152	462.358-521.818
Average	67.990	

Repeated Electron Irradiation before Protein Treatment (Sample D):

This experiment was performed in the same manner as that of Sample C in order to prove its reproducibility. Intensity and homogeneity comparison between this experiment and that of the previous experiment allow for a better understanding of protein affinity to estersils.

As expected the hexagonal arrays were present at several areas indicating the reproducibility for protein adsorption at the electron irradiated areas (Figure 22).

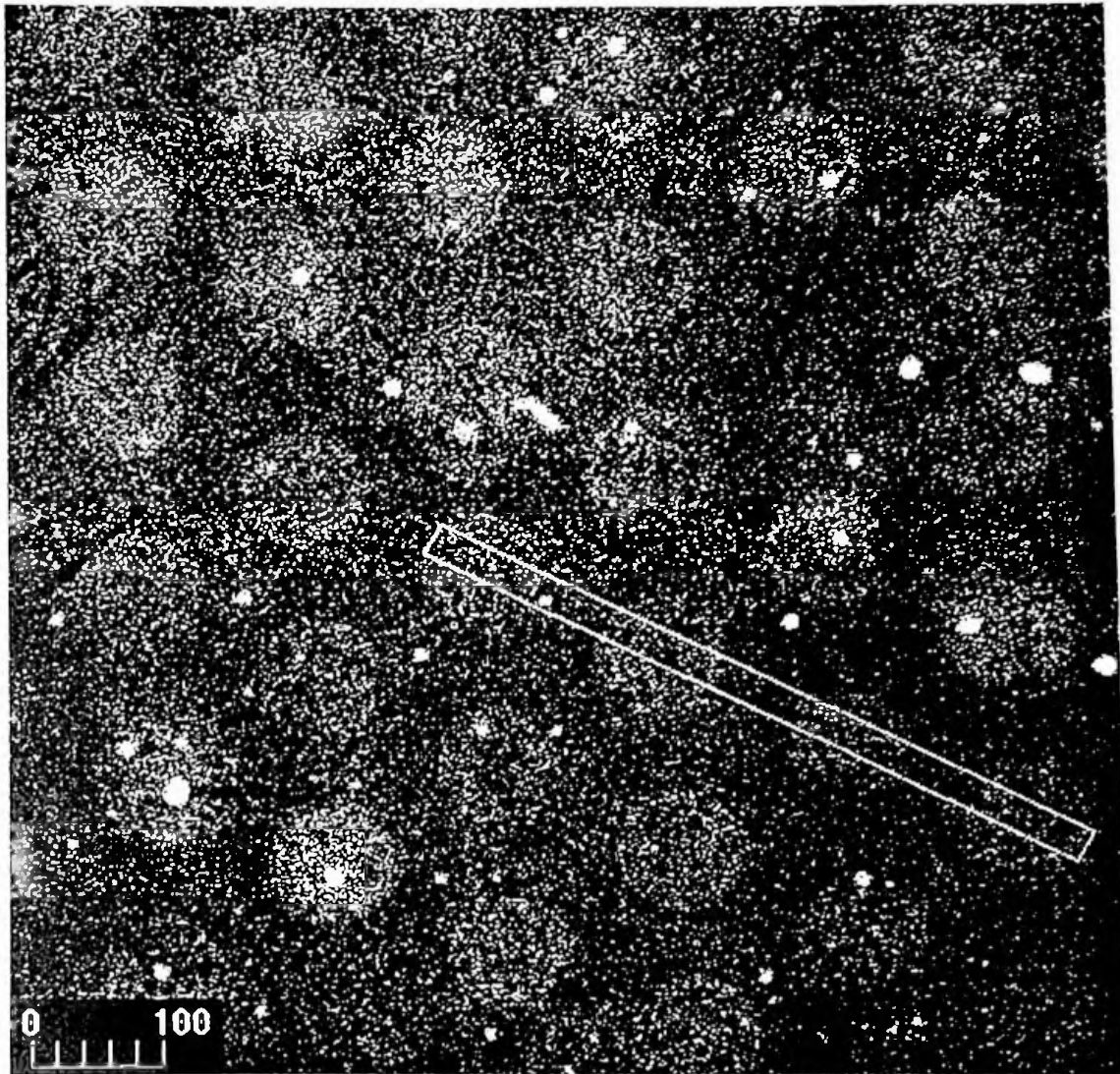


Figure 22. Confocal Micrograph of Sample D. Confocal parameters: averaging = Kalman (2 times), magnification = 10X, wavelength = 488nm, laser power = 100%, iris = 8.0, gain = 1500, B-level = 0, and the low sig. button checked for Mixer A.

Figure 23 is the graph of the line intensity of Sample D. With the help of a 10-point trendline, the graph shows sharp dips in intensity indicating the background.

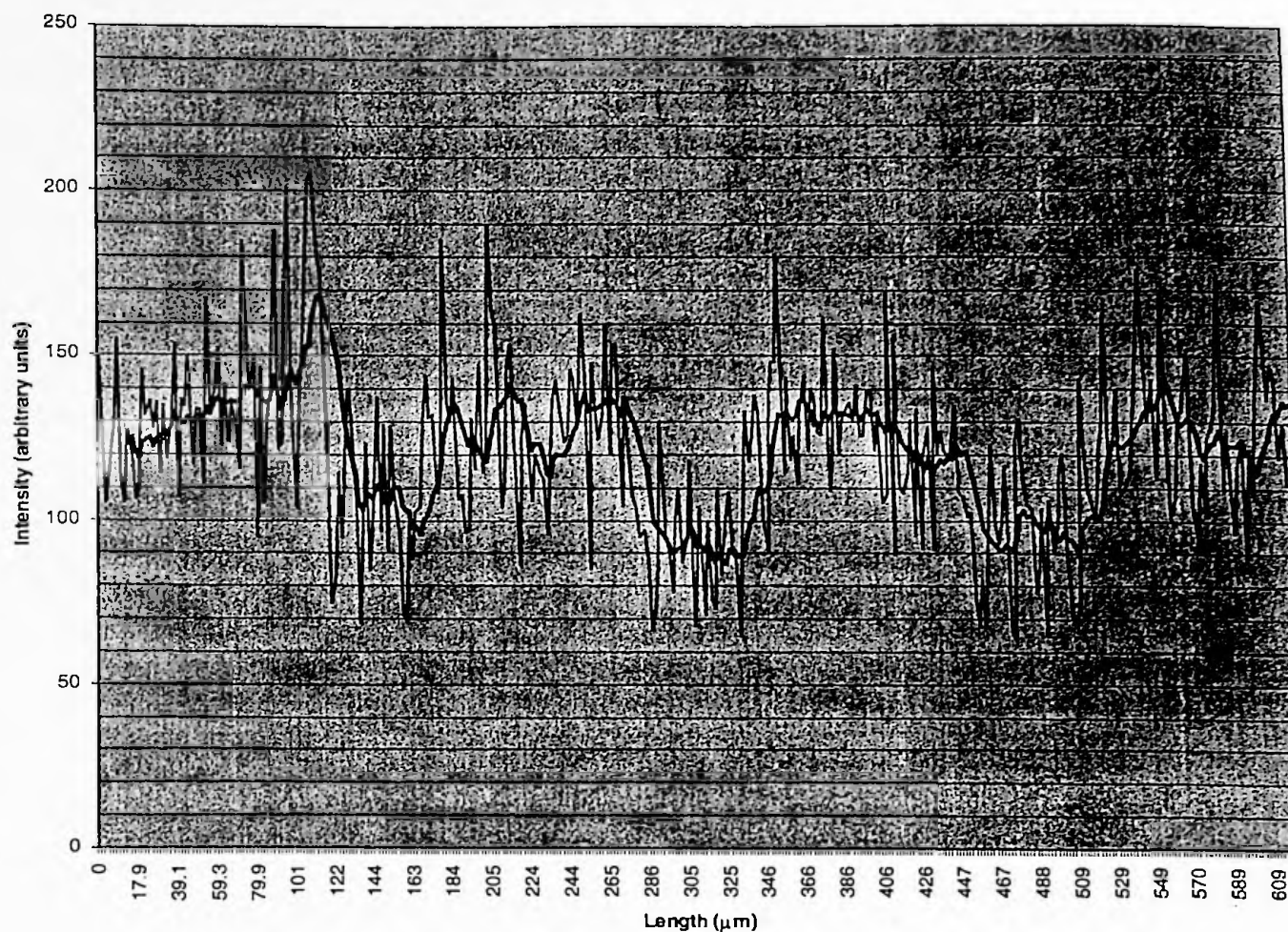


Figure 23. Line Intensity of Sample D. (Light line = raw data) (Dark line = 10 point moving average)

Table 5, also shows the difference between the background and the pattern intensities. Even though the difference in numeric intensity is not as prominent, visually the difference between background and pattern is clear. Again this experiment proves the higher affinity to protein at

irradiated areas where the estersils are broken and lower affinity to areas where the estersils are presumably still present. The signal to background ratio is 1.4.

Table 5. Average Intensities of Sample D

	Avg. Intensity	Length Interval
First pattern	138.079	8.0972-110.87
Second pattern	130.067	180.27-273.68
Third pattern	127.292	355.92-446.957
Fourth pattern	127.617	525.151-601.38
Average	130.764	
First background	102.271	119.95-163.09
Second background	90.359	287.50-333.02
Third background	97.020	459.10-519.42
Average	96.550	

Electron Irradiation before Protein Treatment (Ethanol Flame Dried) (Sample E):

This procedure was identical to the previous experiment (Sample D), however, ethanol was used in place of methanol. This experiment was performed in order to understand the relationship between the degree of esterification with the affinity to protein.

As expected Figure 24 (328g) show similar hexagonal arrays as the methanol flame dried experiments even though ethanol was used.

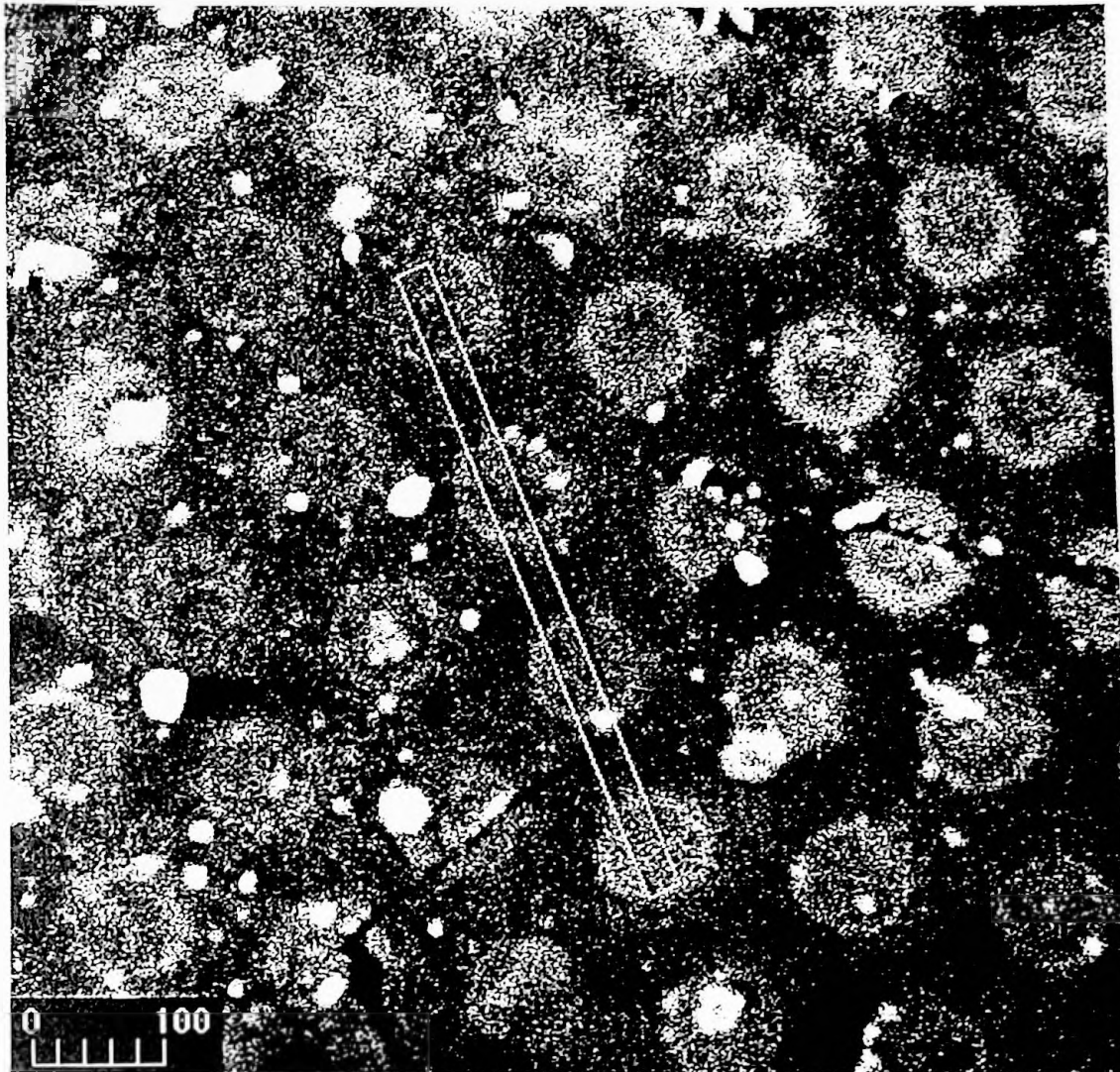


Figure 24. Confocal Micrograph of Sample E. Confocal parameters: averaging = Kalman (2 times), magnification = 10X, wavelength = 488nm, laser power = 100%, iris = 8.0, gain = 1500, B-level = 0, and the low sig. button checked for Mixer A.

The line intensity measured and graphed also indicates clear distinction between the pattern and the background (Figure 25).

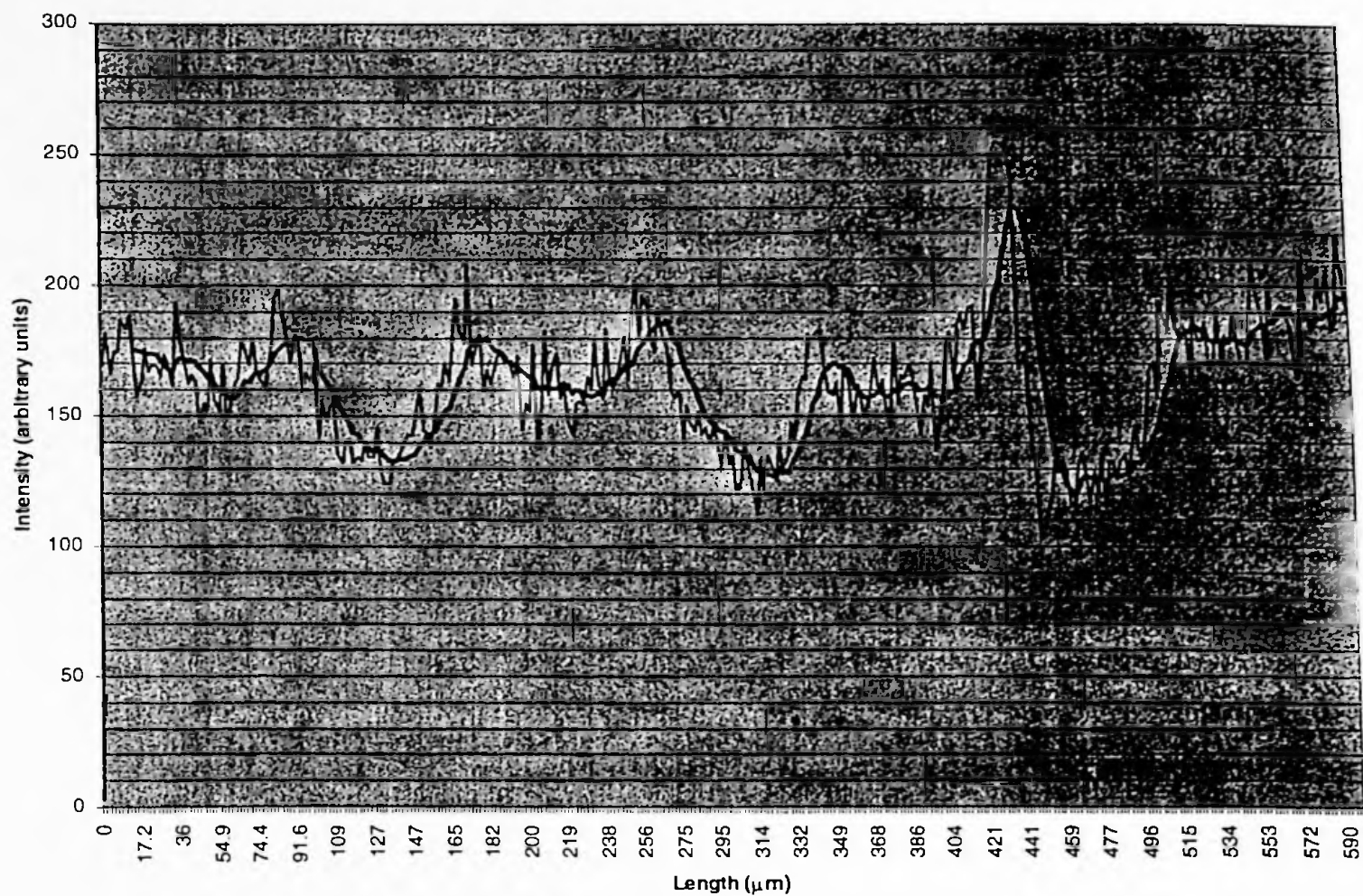


Figure 25. Line Intensity of Sample E. (Light line = raw data) (Dark line = 10 point moving average)

Table 6 is a listing of the calculated average intensity of Sample E, which indicates a definite intensity distinction between pattern and background. The signal to background ratio is 1.3.

Table 6. Average Intensities of Sample E

	Avg. Intensity	Length Interval
First pattern	168.111	9.774-82.531
Second pattern	170.119	168.127-266.158
Third pattern	173.899	340.591-434.980
Fourth pattern	186.445	507.736-591.944
Average	174.643	
First background	139.891	102.079-154.999
Second background	136.253	277.609-331.511
Third background	130.487	447.126-497.962
Average	135.544	

According to Ballard et al., methanol has the highest degree of esterification, which decreases with higher alcohols such as ethanol, propanol, butanol, etc.²¹ One can see by comparing the average background intensities of Sample C, Sample D, and Sample E, that the Sample E background intensity is higher than the other background intensities. The reasoning is that since ethanol has a lower degree of esterification it does not completely cover the treated coverslip allowing for the proteins to adhere to areas that are not bombarded with electrons.

Blank Experiment without Methanol (Sample F):

This experiment was performed as a blank. A coverslip was kimwipe cleaned (no alcohol flaming) and placed under the SEM for electron irradiation through the mask. Two areas were irradiated with electrons at the standard SEM parameters. After the irradiation, the estersil free coverslip was not treated with any protein but rather immediately observed under the confocal at the standard confocal parameters.

This blank experiment was expected to show no observable fluorescent patterns, only random specks of fluorescent or a dark background was expected. However, contrary to the expectation, clear patterns were observed. Visually the patterns are well defined, however, the contrast at the center of each patterns is not very different from the background (Figure 26).

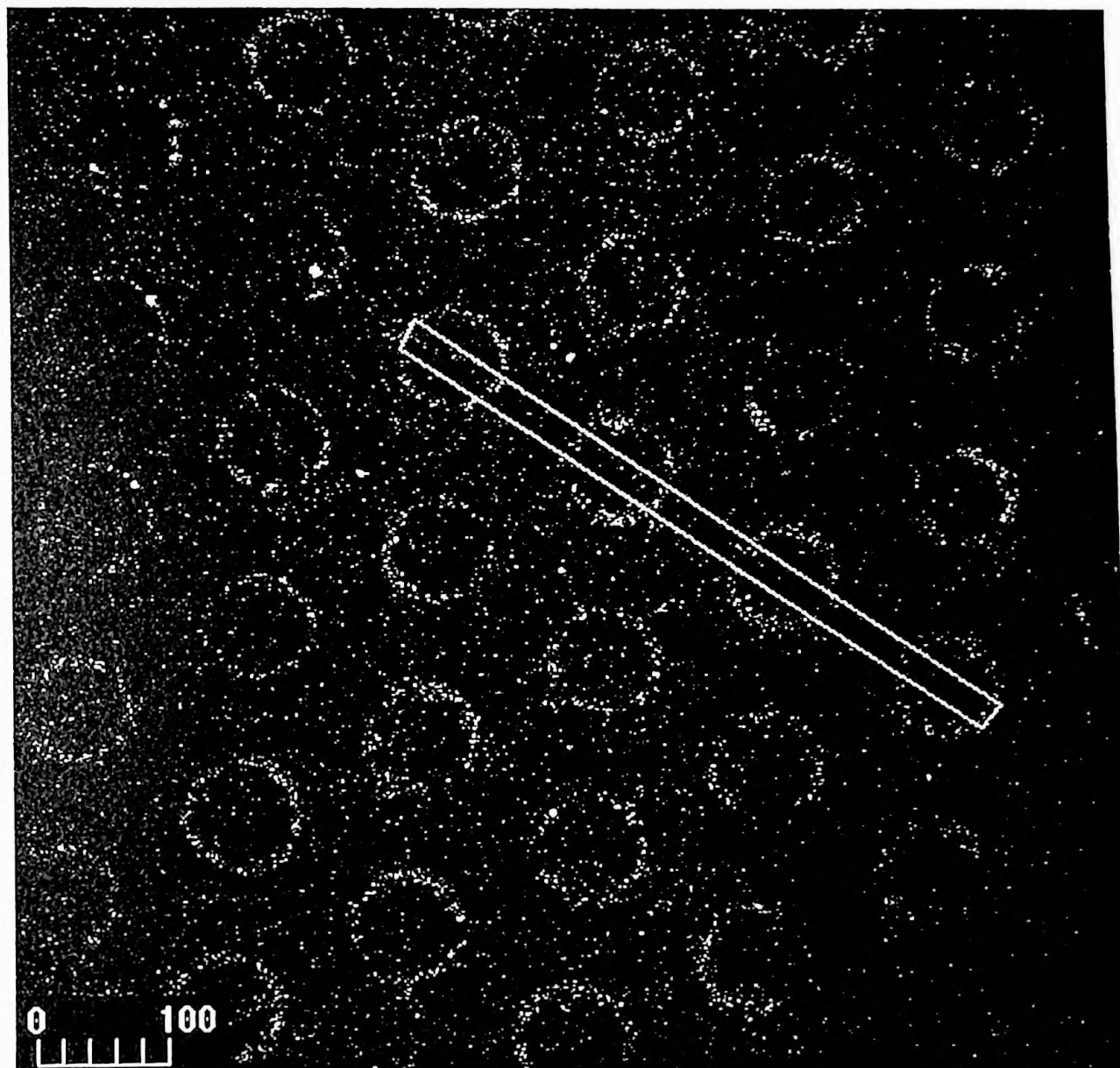


Figure 26. Confocal Micrograph of Sample F. Confocal parameters: averaging = Kalman (2 times), magnification = 10X, wavelength = 488nm, laser power = 100%, iris = 8.0, gain = 1500, B-level = 0, and the low sig. button checked for Mixer A.

The line intensity graph (Figure 27) does show that there is no great distinction between the background and the pattern intensities at the center of each feature.

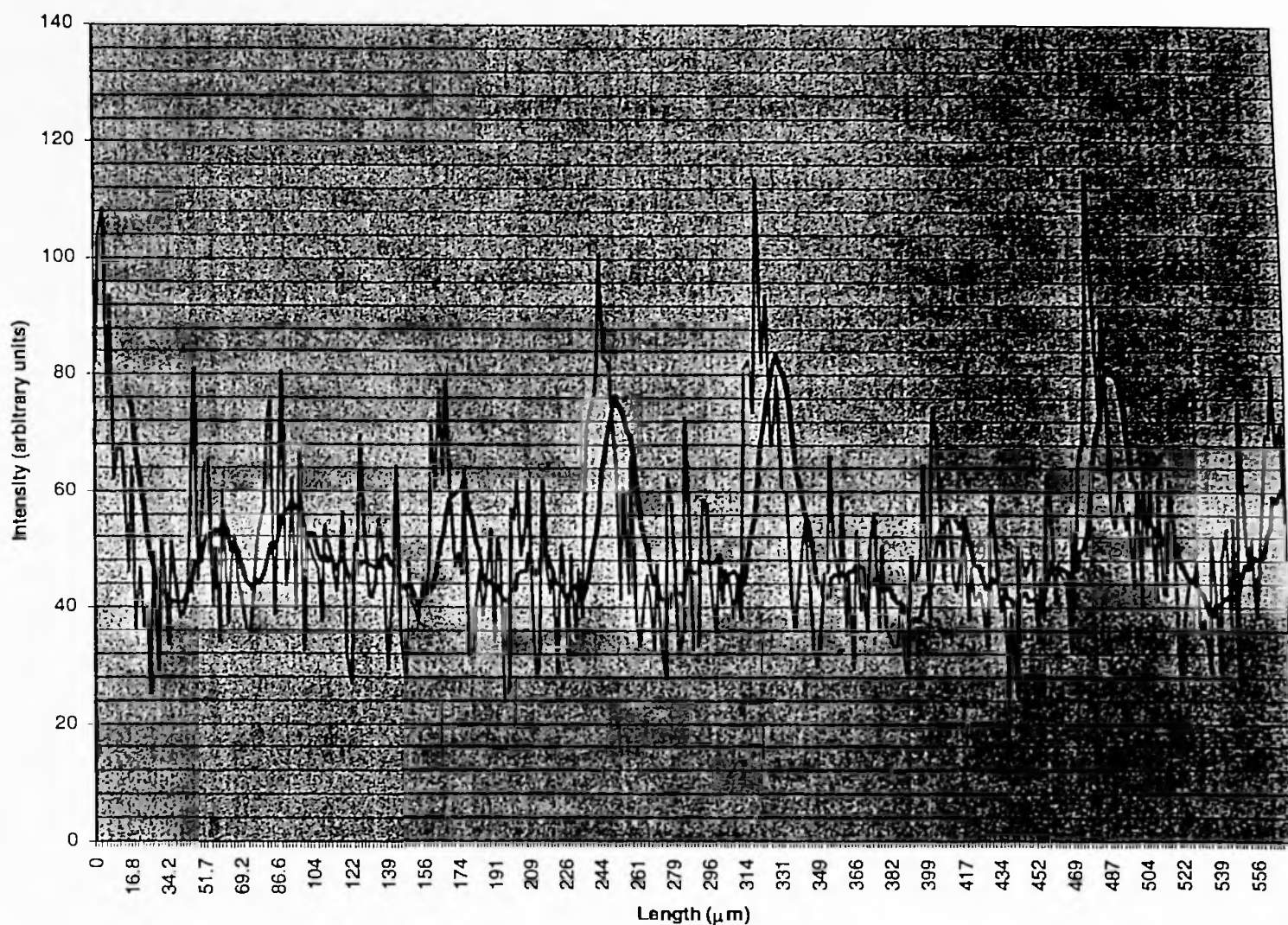


Figure 27. Line Intensity of Sample F. (Light line = raw data) (Dark line = 10 point moving average)

The higher intensity of the rings observed around each pattern is prominent in this graph with sharp increase in intensity. Table 7, calculated values shows that the average intensity of the patterns and backgrounds are relatively low and not significantly different from each other compared to the other experiments (Sample C, D, and E). The signal to background ratio is 1.2.

Table 7. Average Intensities of Sample F

	Avg. Intensity	Length Interval
First pattern	52.230	3.354-88.305
Second pattern	52.533	162.213-248.841
Third pattern	52.385	315.346-404.346
Fourth pattern	53.639	480.913-566.559
Average	52.697	
First background	45.627	95.708-154.81
Second background	44.037	262.952-311.992
Third background	43.669	415.103-469.174
Average	44.444	

So if the rings were not present, no patterns would have been observed and therefore this would be a useful blank. The high contrast ring around each pattern is proposed to be due to sputtering of the nickel mask onto the coverslip. SEM X-ray analysis did not indicate nickel on this substrate. However, the nickel level may be below the detection limit. Another test of this theory requires that a maskless experiment needs to be performed, as described on page 60 below.

Blank Experiment with Methanol (Sample G):

In this case, the coverslip was flame dried with methanol and irradiated with electrons through the mask in two areas using standard SEM parameters. After the irradiation, the coverslip was removed and again was not treated with protein. Images were captured using standard confocal parameters.

Once again hexagonal patterns were not expected to be observed in this blank experiment. Conflicting with expectation, patterns were observed (Figure 28).



Figure 28. Confocal Micrograph of Sample G. Confocal parameters: averaging = Kalman (2 times), magnification = 10X, wavelength = 488nm, laser power = 100%, iris = 8.0, gain = 1500, B-level = 0, and the low sig. button checked for Mixer A.

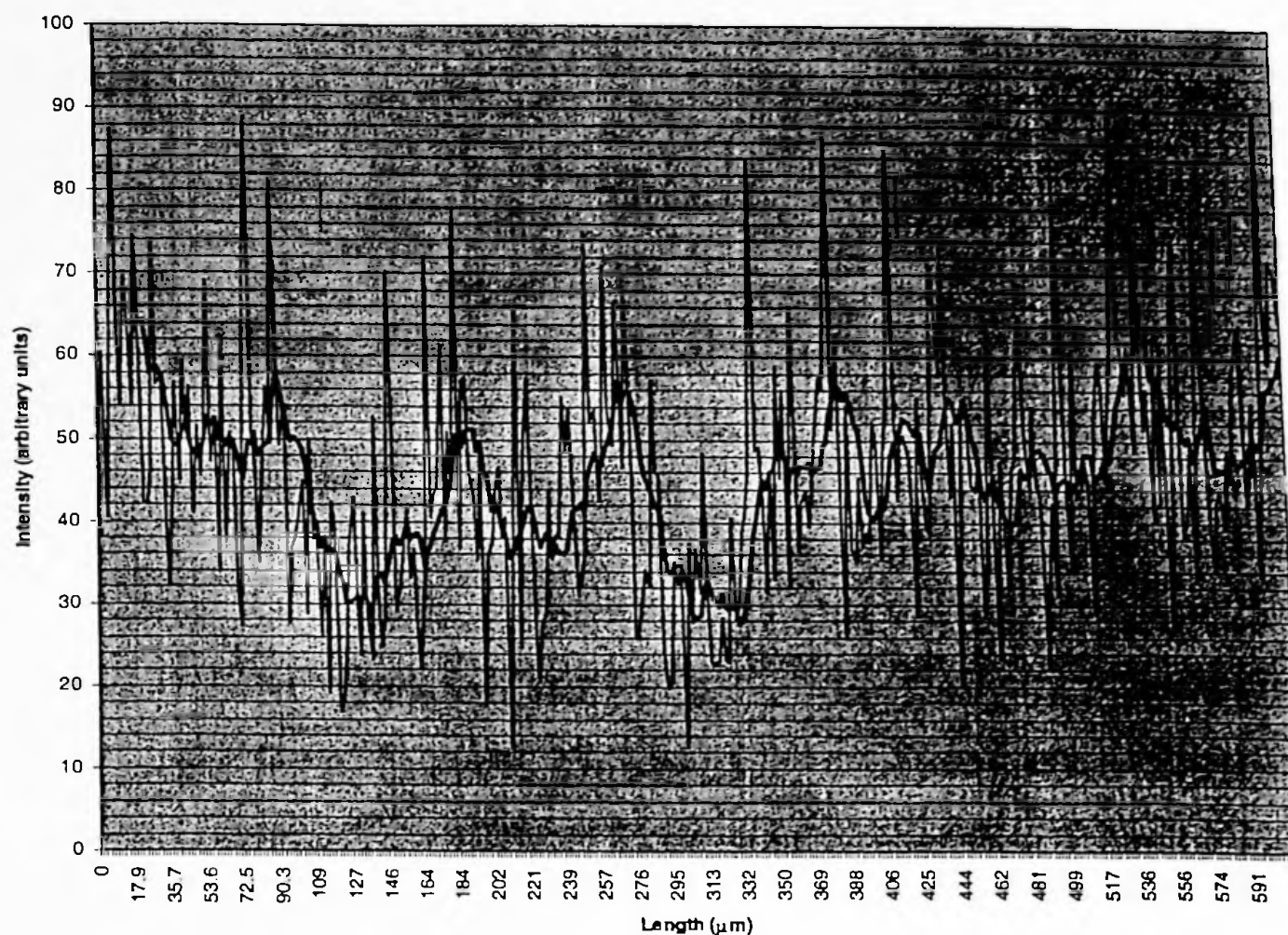


Figure 29. Line Intensity of Sample G. (Light line = raw data) (Dark line = 10 point moving average)

There are some sharp peaks visible in the graphed line intensity profile (Figure 29), which represent the rings around the patterns. As in the previous experiment, the background average intensity is not very different from the average intensity of the patterns. Also their overall intensities are not very high, lower than 100 (Table 8). The signal to background ratio is 1.4.

Table 8. Average Intensities of Sample G

	Avg. Intensity	Length Interval
First pattern	53.460	3.354-88.305
Second pattern	45.566	162.213-248.841
Third pattern	50.217	315.346-404.346
Fourth pattern	53.992	480.913-566.559
Average	50.809	
First background	34.498	95.708-154.81
Second background	31.836	262.952-311.992
Third background	44.463	415.103-469.174
Average	36.932	

Electron irradiation does appear to render the surface fluorescent. Irradiated glass may luminescence. Another possibility is that sputtering of the mask onto the coverslip produces a fluorescent material. However, with the treatment of protein as in Sample B, C, and D the intensity of the patterns does increase. Therefore, one can ask whether the sputtered material (NiO) also increases the affinity of protein to that area. The maskless experiments described next eliminate any mask derived artifacts. Therefore, they allow us to explore the possibility that sputtering of the mask may be the cause of not only the fluorescent rings but also the increase in affinity of protein to the irradiated areas.

Maskless Experiments:

Testing a Program for Generating Patterns by Electron Beam Direct Write using a KBr crystal (Sample H):

This experiment was performed to test the DACTA computer program and the mechanical system for use in maskless experiments. A KBr crystal was mounted on a SEM stub with double-sided carbon tape. The crystal was irradiated with electrons using a new set of SEM parameters. The exposure time was varied by the program used (Matrix) and a higher magnification (X1500) was used to mimic the 90- μm spot. Characteristic F- colors or centers (blue) can be induced in KBr with high-energy electron irradiation.

The blue color results from the excitation of the electron in a halide ion vacancy.²³

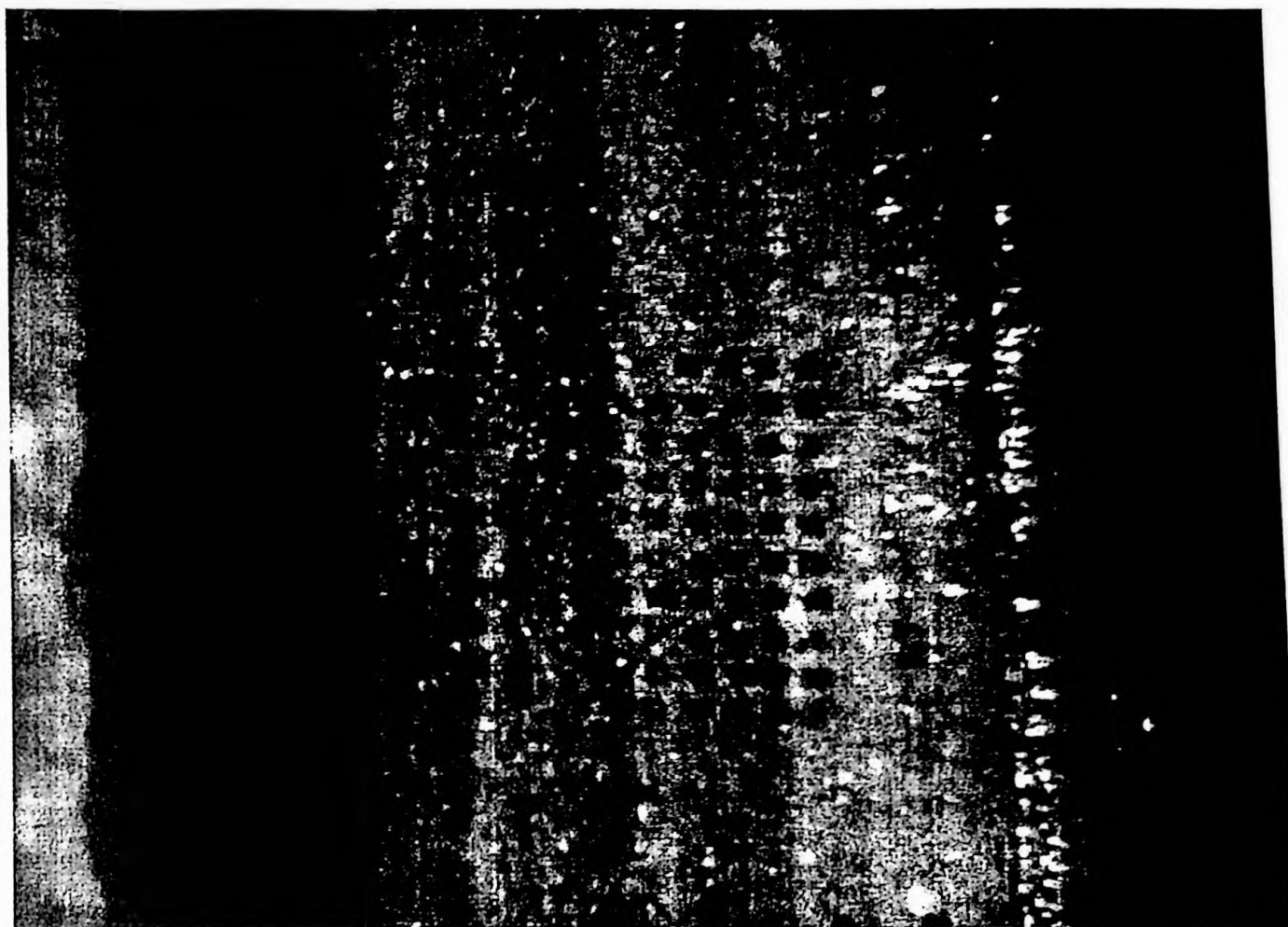


Figure 30. Electron Beam Direct Write Pattern on a KBr Crystal. The blue color is a result of F-centers. SEM parameters: time of exposure = varied from 0.1 sec, 0.5 sec, 1 sec, 5 sec, 10 sec, 15 sec, 30 sec, 60 sec and 5 min blockers at each side, acceleration voltages = 30kV, magnification = X1500, spot size 24, working distance (wd) = 20, and load current = 98 μ A.

As expected, a matrix of bluish patterns were observed with a dissecting microscope (Figure 30). This result demonstrates that it is possible to use the DACTA control system

to reproducibly translate the SEM stage. Electron beam writing experiments on the coverslip were then performed.

Electron Beam Direct Write on Coverslip (Sample I):

This experiment was performed to confirm that mask sputtering is the cause for the background fluorescence in Samples F and G. This experiment mimics the other protein free blank experiments that used a nickel mask. In order to accomplish this task, a magnification was determined (X1500) to best represent a single 90- μm spot. To assure equal electron exposure at X1500 as at X35, the Dosage formula was used. Setting $\text{Dose}_{\text{low mag.}} = \text{Dose}_{\text{high mag.}}$ with current set at 98- μA on both sides, and the magnification set at X35 with a time of 30 minutes for the $\text{Dose}_{\text{low mag.}}$ side. For the $\text{Dose}_{\text{high mag.}}$ side, the magnification is X1500. "Time" for the high magnification side was found to be 0.98 sec. The Matrix1 program was used to electron write on a methanol flame dried coverslip at the SEM direct write parameters for 0.98 seconds at X1500.

This experiment was expected to yield a 6X8 array of fluorescent patterns if electron irradiation alone produced fluorescence. Contrary to this expectation, no patterns were observed (Figure 31).

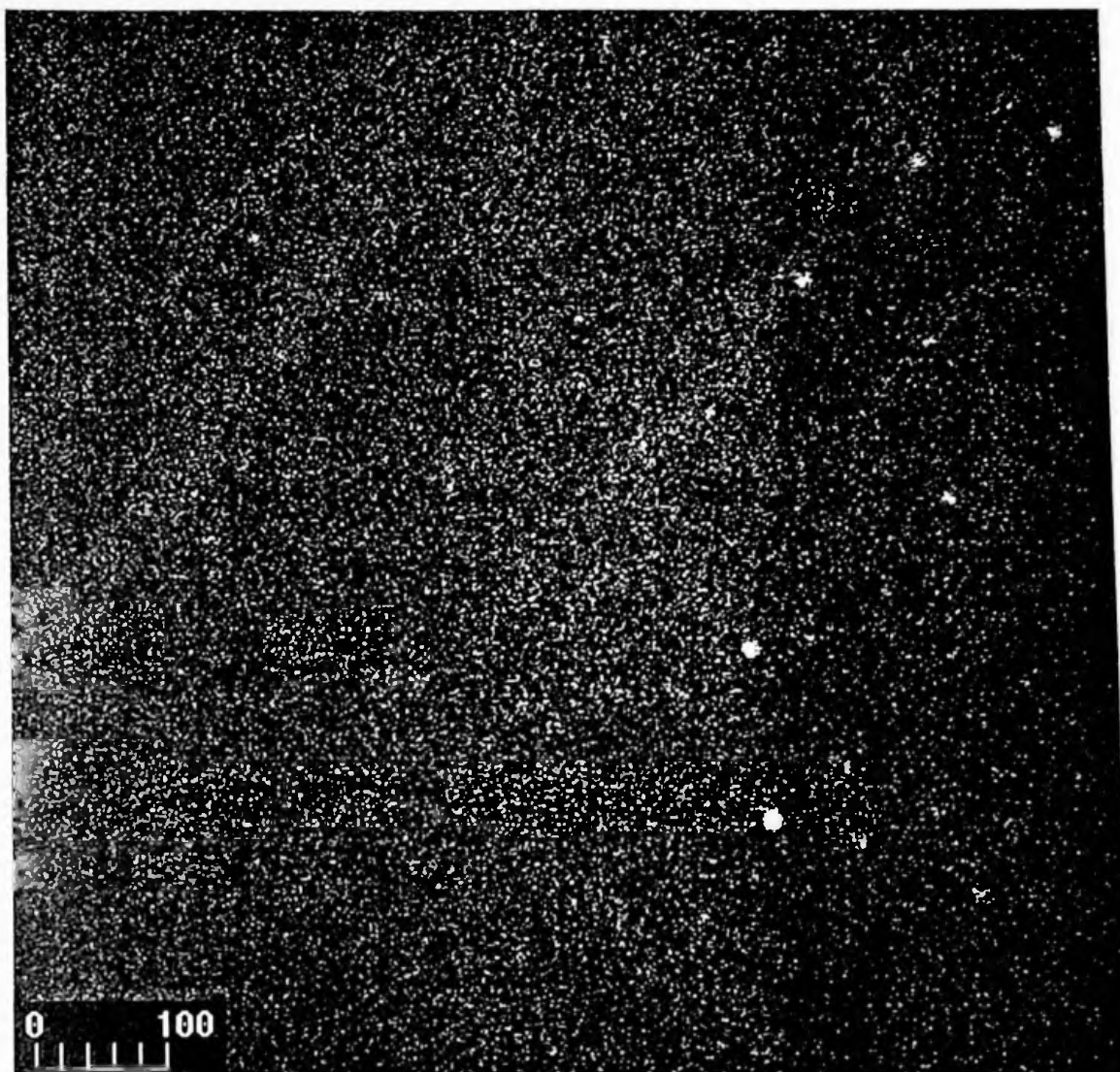


Figure 31. Confocal Micrograph of Sample I. Confocal parameters: averaging = Kalman (2 times), magnification = 10X, wavelength = 488nm, laser power = 100%, iris = 8.0, gain = 1500, B-level = 0, and the low sig. button checked for Mixer A.

Another explanation for the protein patterning observed must be formulated. The only difference between this experiment and that of Samples F and G is that in those experiments a mask was used. One explanation could be sputtering of the nickel mask. This is supported by the two blank mask experiments (Sample F and G). Those two

blank substrates were not treated with any protein or antibody, yet still showed fluorescence. It is possible that the electron beam sputtered nickel oxide (NiO), which is fluorescent, onto the glass surface (Samples F and G). The sputtered material also increases the affinity of protein in these areas hence the patterns are more intense (Sample A, C, D, and E).

Nickel oxide displays photoluminescence emission in the 3.5 to 2.1 eV (350 to 600 nm) spectral range according to Diaz-Guerra et. al.²⁴ They were interested in the direct comparison of the cathodoluminescence and photoluminescence emission in the visible and near IR ranges of nickel oxide. Figure 32 displays their photoluminescence spectra for NiO at different temperatures.²⁴

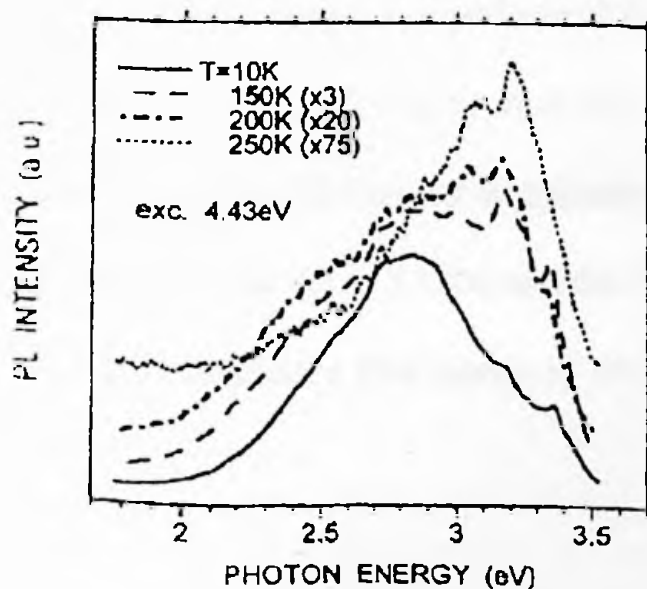


Figure 32. NiO Photoluminescence Spectra (excitation = 280 nm)

Using the formula $E = (h \cdot c) / \lambda$, where $(h \cdot c) = 1.239 \times 10^{-4} \text{ eV} \cdot \text{cm}$, the energy at which fluorescence was observed using the confocal microscope (598 nm) was

calculated. The energy was found to be 2.072 eV. According to Diaz-Guerra et. al, NiO should display some fluorescence emission intensity at this wavelength. This further supports the contention that sputtering of the nickel mask was the cause for the fluorescent ring patterns in the two blank experiments (Sample F and G). A ring pattern would be expected since the majority of sputtered material would be remaining near the Ni mask.

Testing A New Program to Investigate Irradiation Time Dependence Using KBr Crystal (Sample J):

This experiment was performed to test a program, which would vary the irradiation time for different spots in the matrix before it was used in the coverslip experiments. The KBr crystal was irradiated at standard SEM parameters, except the magnification was set at X1500 and the time was varied by the program (Matrix2).

As expected, a 9X4 matrix of bluish spots were observed (Figure 33).

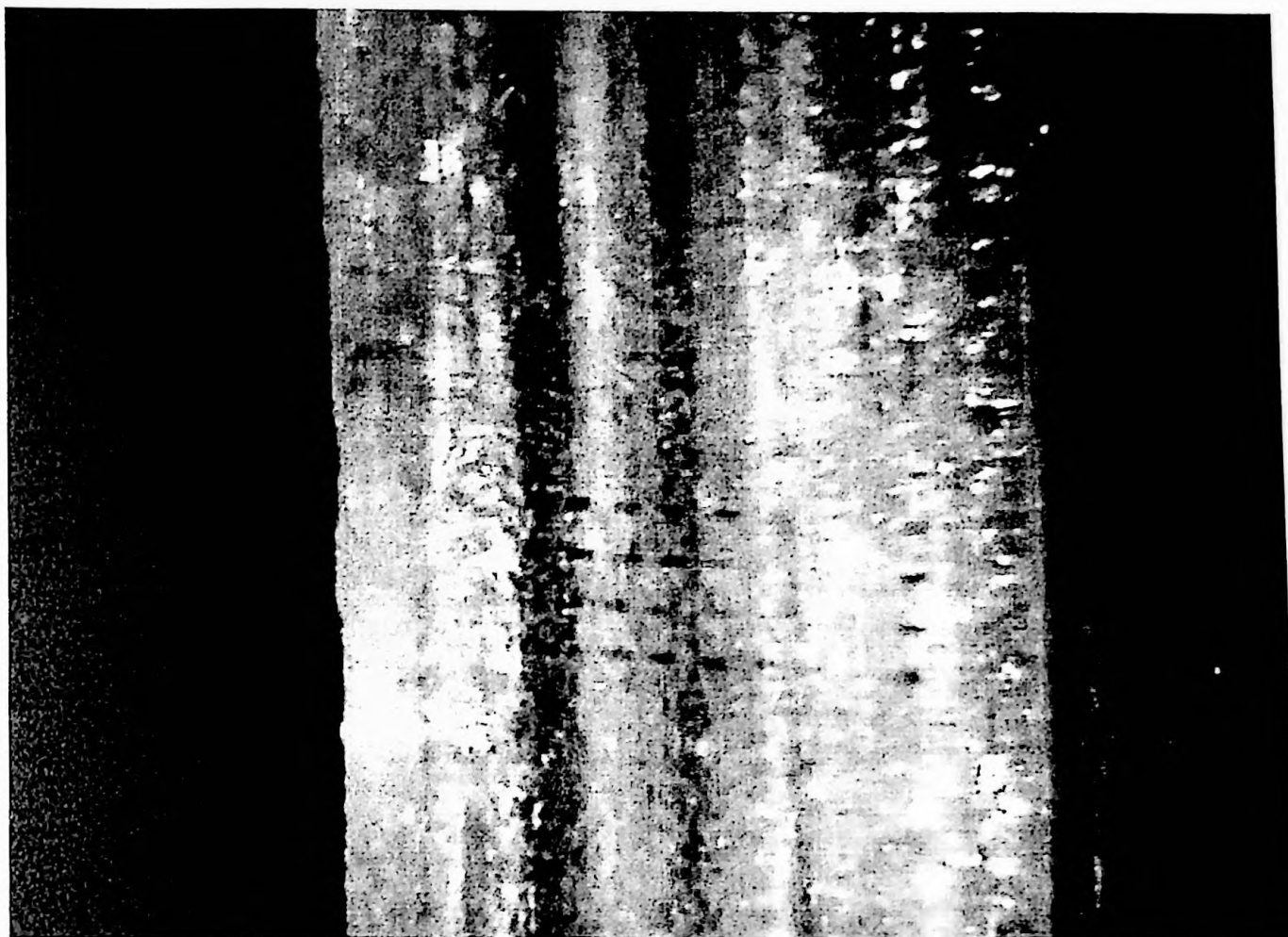


Figure 33. Electron Beam Direct Write Pattern on a KBr Crystal used to Check DACTA program. The blue color is a result of F-centers. SEM parameters: time of exposure = varied from 0.5 sec, 0.98 sec, 5 sec, 10 sec, 15 sec, 30 sec, 60 sec and 5 min blockers at each side, acceleration voltages = 30kV, magnification = X1500, spot size 24, working distance (wd) = 20, and load current = 98 μ A.

The patterns are rectangular because slow line scan mode was used instead of the TV mode, which gave the square patterns observed in Sample H. Now that the program has been shown to work on the KBr crystal, similar exposure will be produced on coverslips.

Time of Exposure Versus Intensity without antibody (Sample K):

Short-term direct electron irradiation does not appear to induce substrate fluorescence. This experiment was performed to determine the relationship between the time of exposure and the intensity of fluorescence observed without antibody. Five-minute exposure times were used on each side of the matrix in order to define the boundaries and in order to identify where the exposure time starts and ends. The Matrix2 program was used at the standard SEM parameters however, the magnification was set at X1500. The coverslip was flame dried with methanol before electron irradiation. It was not treated with antibody but immediately observed under the confocal at standard confocal parameters.

As seen in Figure 34, direct electron writing does produce significant fluorescence at long exposure times.

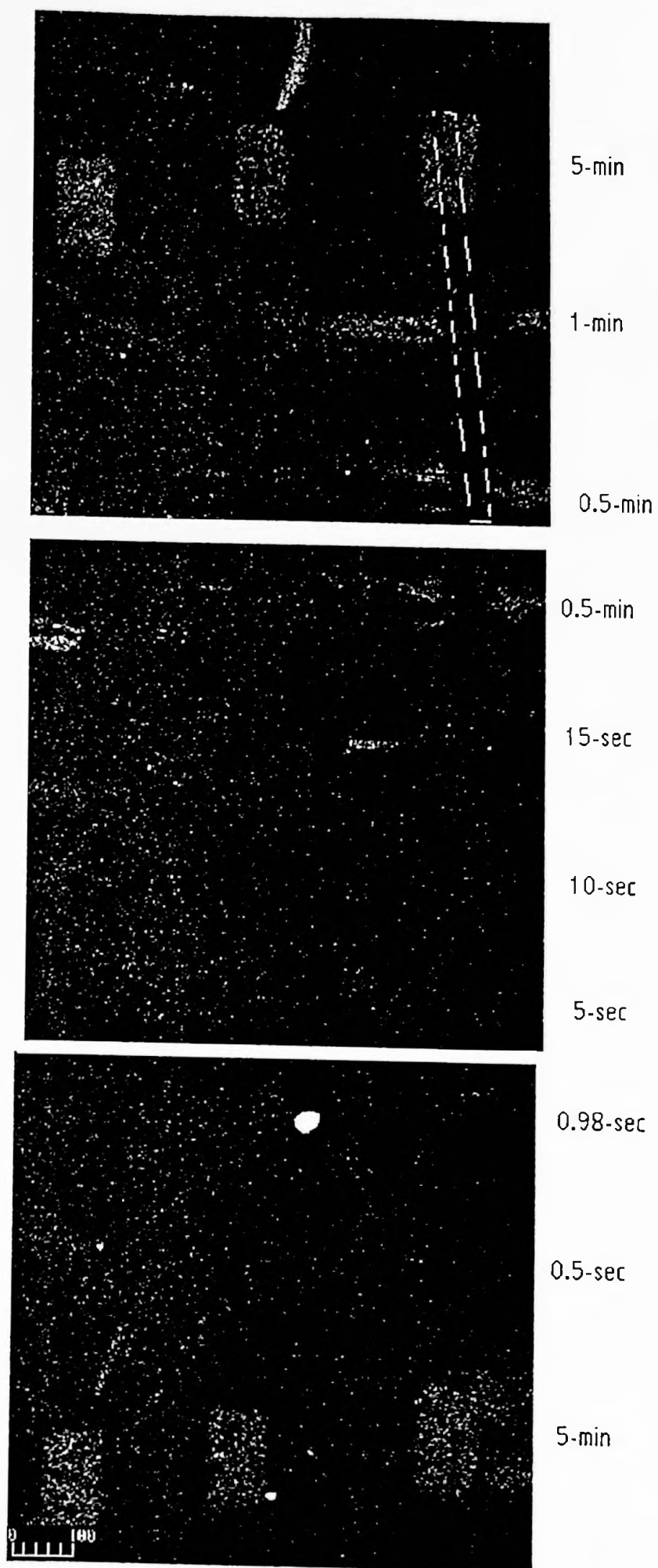


Figure 34. Confocal Micrographs of Sample K. Confocal parameters: averaging = Kalman (2 times), magnification = 10X, wavelength = 488nm, laser power = 100%, iris = 8.0, gain = 1500, B-level = 0, and the low sig. button checked for Mixer A.

The observation that electron beam direct write does show fluorescent is represented best at the longer exposure times (5 min, 1 min and 0.5 min). At the 0.98-sec mark (equivalent to 30-min irradiation at X35) there is no observable fluorescence. This indicates that electron irradiation of the coverslip has no significant contribution to the fluorescent patterns observed in the blank experiments (Sample F and G) and that mask sputtering is the cause for the observed fluorescence.

The measured line intensity across the three patterns of Figure 34 was graphed in Figure 35.

Figure 35. Line intensity of Figure 34. (The line intensity is plotted as a function of position across the three patterns.)

The line intensity is plotted as a function of position across the three patterns. The line intensity is plotted as a function of position across the three patterns. The line intensity is plotted as a function of position across the three patterns.

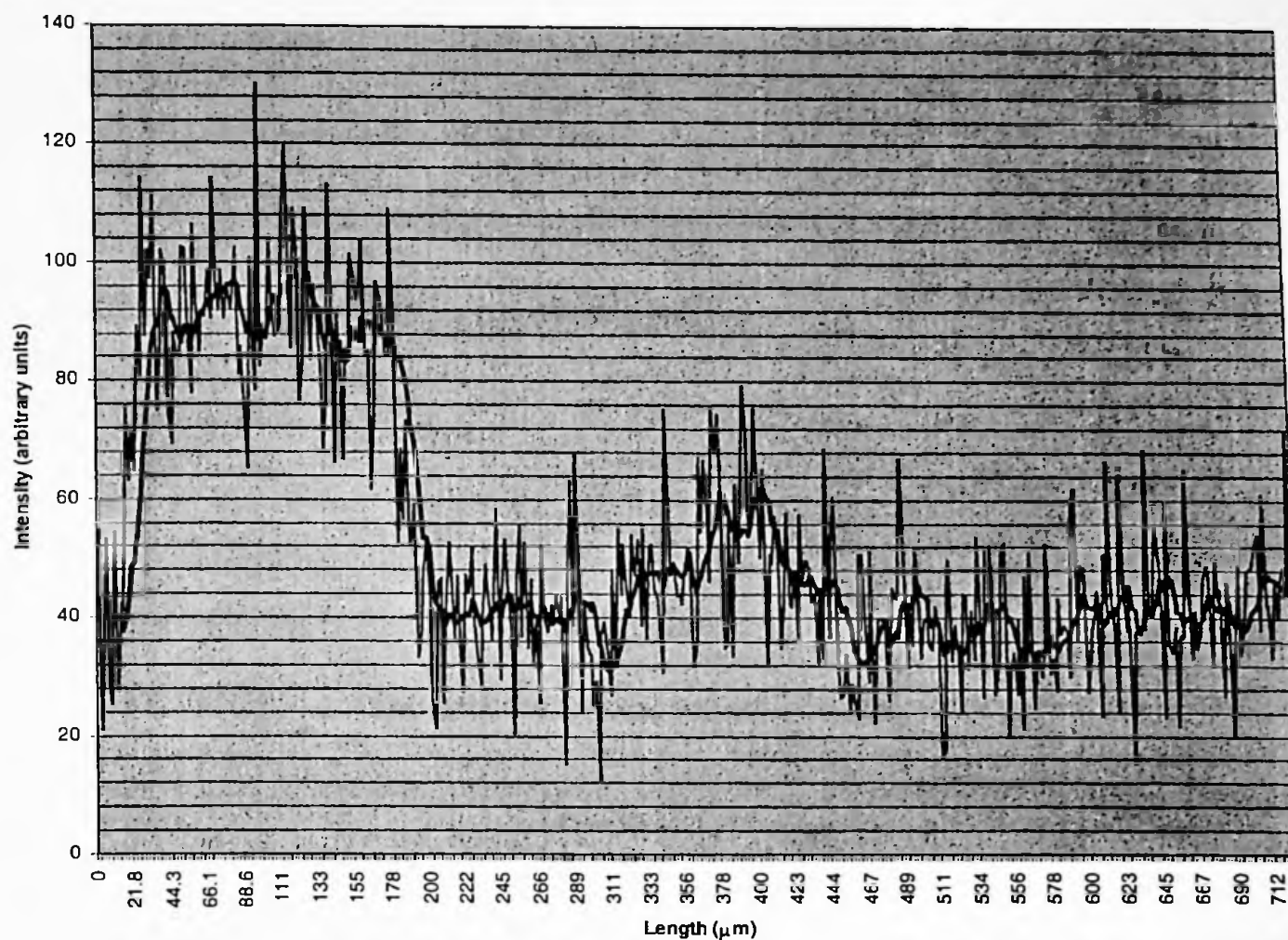


Figure 35. Line Intensity of Sample K. (Light line = raw data) (Dark line = 10 point moving average)

The first pattern and second patterns are clearly more intense than the background intensity. The third pattern is almost indistinguishable from the background.

Table 9 lists the calculated average intensities of the patterns and background of Figure 34. Once again the intensities between the patterns and the backgrounds are distinguishable.

Table 9. Average Intensities of Sample K

	Avg. Intensity	Length Interval
First pattern	89.207	16.770-186.266
Second pattern	47.275	314.820-487.670
First background	39.662	192.974-309.094
Second background	36.736	499.409-590.374

This experiment shows that electron beam direct write does cause fluorescence, but at much longer exposure times than those employed in the mask experiments. The next experiment will test the electron beam direct write patterns affinity toward protein.

Treating Sample K with FITC antibody (Sample L):

This experiment simply involves taking Sample K and treating with the FITC secondary antibody and incubating it at room temperature for 1-hr. After the hour, the sample was thoroughly rinsed with deionized water and was observed at standard confocal parameters.

This experiment was conducted to see if electron beam direct write would increase protein adhesion. Visually, there does seem to be a slight increase in fluorescence (Figure 36).

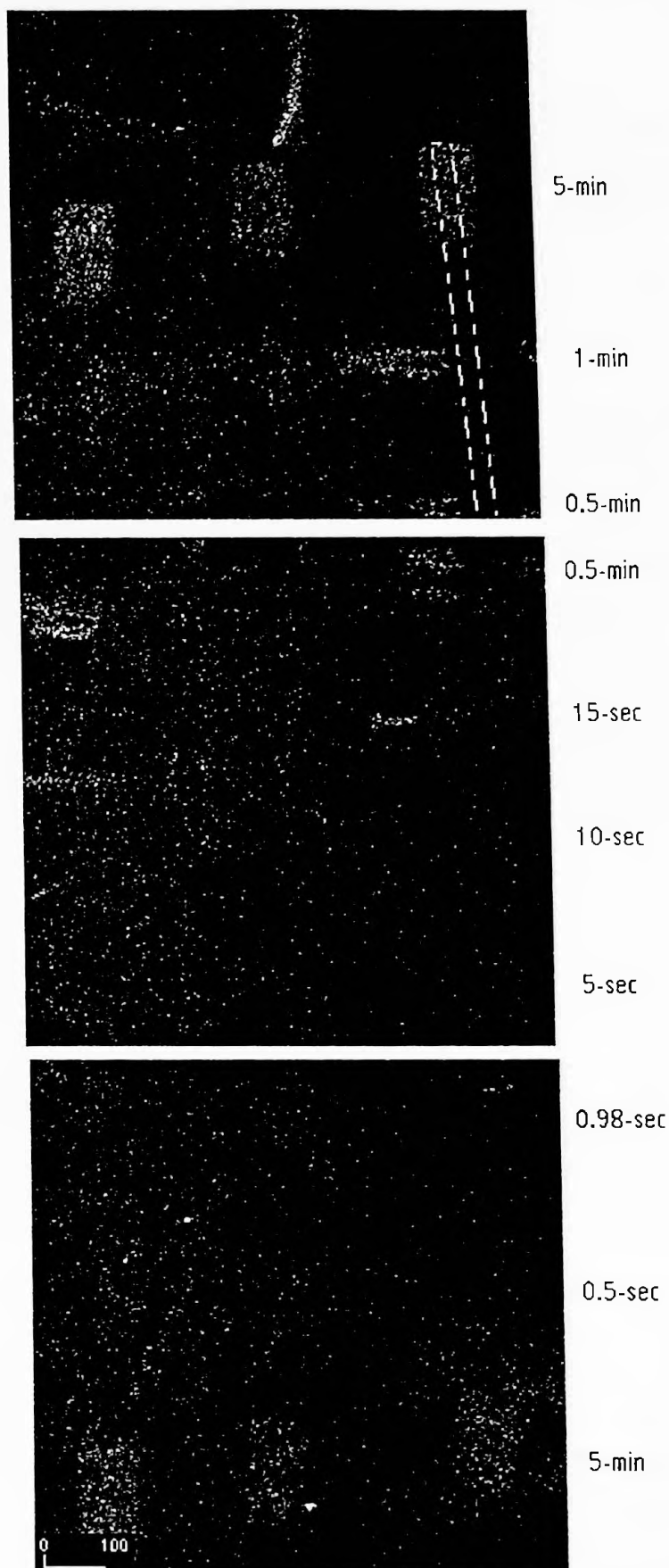


Figure 36. Confocal micrographs of Sample L. Confocal parameters: averaging = Kalman (2 times), magnification = 10X, wavelength = 488nm, laser power = 100%, iris = 8.0, gain = 1500, B-level = 0, and the low sig. button checked for Mixer A.

According to the line intensity graph (Figure 37) there is an increase in fluorescence at the higher exposure times (5-min, 1-min).

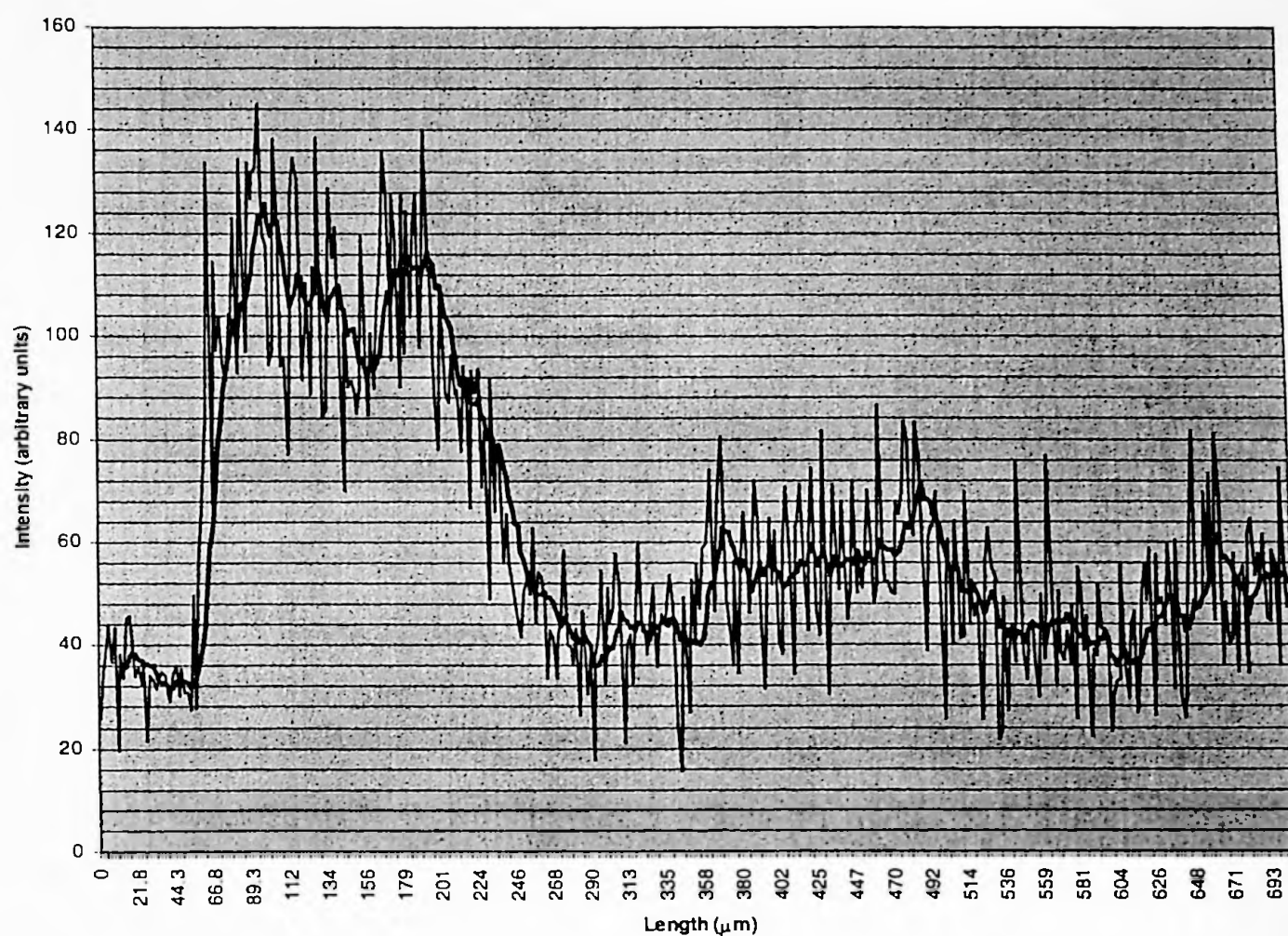


Figure 37. Line Intensity of Sample L. (Light line = raw data) (Dark line = 10 point moving average)

The increase in fluorescence is made even clearer by comparing the calculated average intensities of the observable patterns of this experiment (Table 10) to those of Sample K.

Table 9. Average Intensities of Sample K

	Avg. Intensity	Length Interval
First pattern	89.207	16.770-186.266
Second pattern	47.275	314.820-487.670
First background	39.662	192.974-309.094
Second background	36.736	499.409-590.374

Table 10. Average Intensities of Sample L

	Avg. Intensity	Length Interval
First pattern	102.596	65.115-240.337
Second pattern	58.302	362.877-497.156
First background	42.835	249.417-352.121
Second background	42.975	500.51-615.648

For five-minute exposure, the increase in average signal is $[(102.596 - 89.207) / 89.207] * 100 = 15 \%$.

Short (One-Second) Electron Irradiation of Masked Coverslip under the Nickel Grid (without antibody) Sample M.

This experiment was performed to determine whether a one-second-electron irradiation of the nickel mask at a magnification of X1500 would deposit fluorescent material on the coverslip. A coverslip was flame dried, mounted on the SEM stub and prepared for electron irradiation. Standard SEM parameters were used for the electron irradiation at a magnification of X1500. A 10X20 matrix of holes was irradiated skipping every other row.

A faint pattern with every other row missing was observed (Figure 38). The fact that a visible pattern is observed even at a short exposure time indicates that sputtering of the nickel mask is responsible for much of the luminescence observed in the masked blank experiments. The ring-like appearance of the structures in Figure 38 also is consistent with heterogeneous sputtering, rather than homogeneous electron irradiation of the glass substrate.

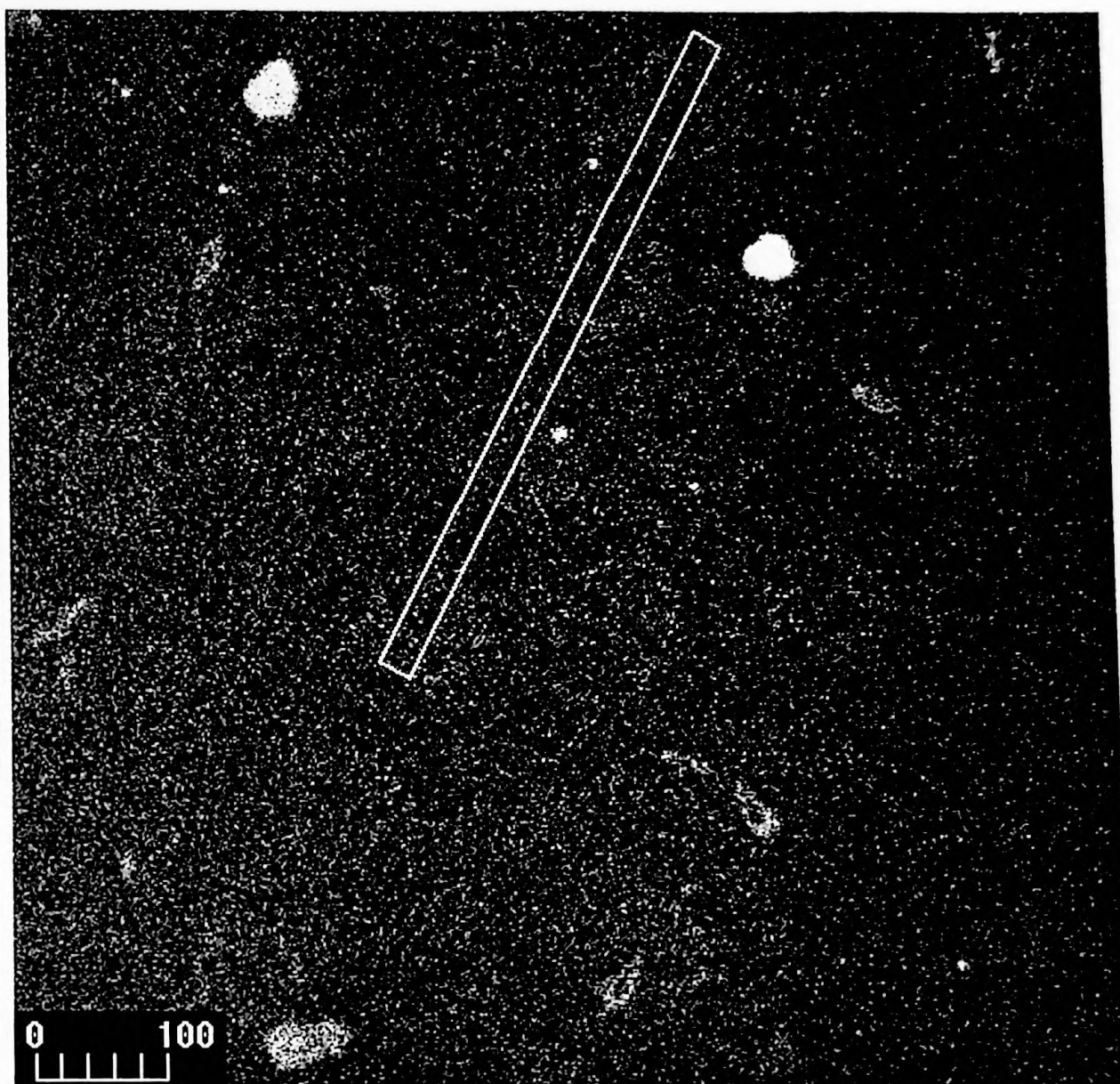


Figure 38a. Confocal Micrograph of Sample M. Confocal parameters: averaging = Kalman (2 times), magnification = 10X, wavelength = 488nm, laser power = 100%, iris = 8.0, gain = 1500, B-level = 0, and the low sig. button checked for Mixer A.

Figure 38a is the same confocal micrograph as Figure 38, however, the contrast was increased to enhance the patterns.

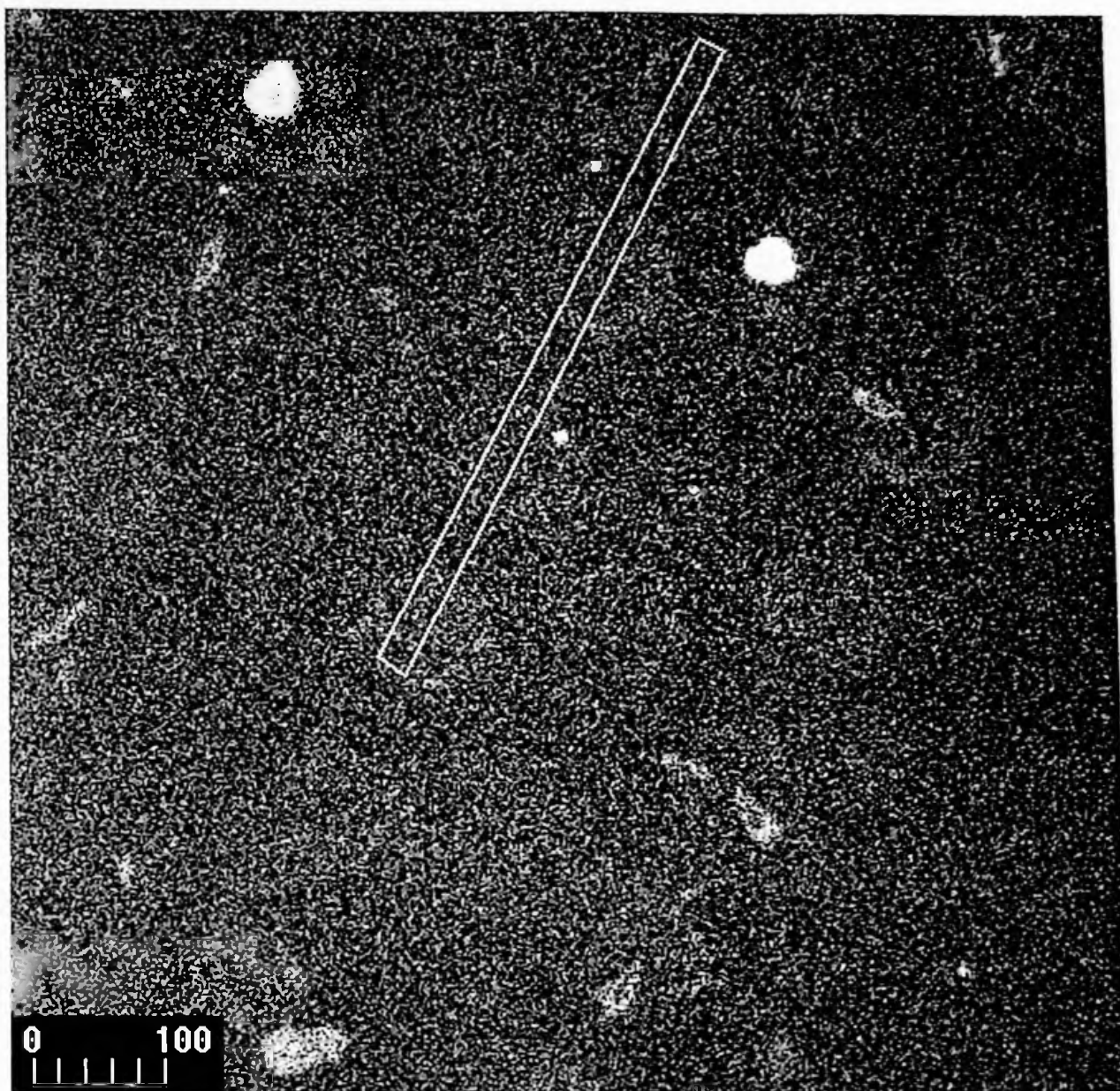


Figure 38b. Confocal Micrograph of Sample M, with increase in Contrast. Confocal parameters: averaging = Kalman (2 times), magnification = 10X, wavelength = 488nm, laser power = 100%, iris = 8.0, gain = 1500, B-level = 0, and the low sig. button checked for Mixer A.

The line intensity across four patterns was measured and the resultant intensities are graphed in Figure 39.

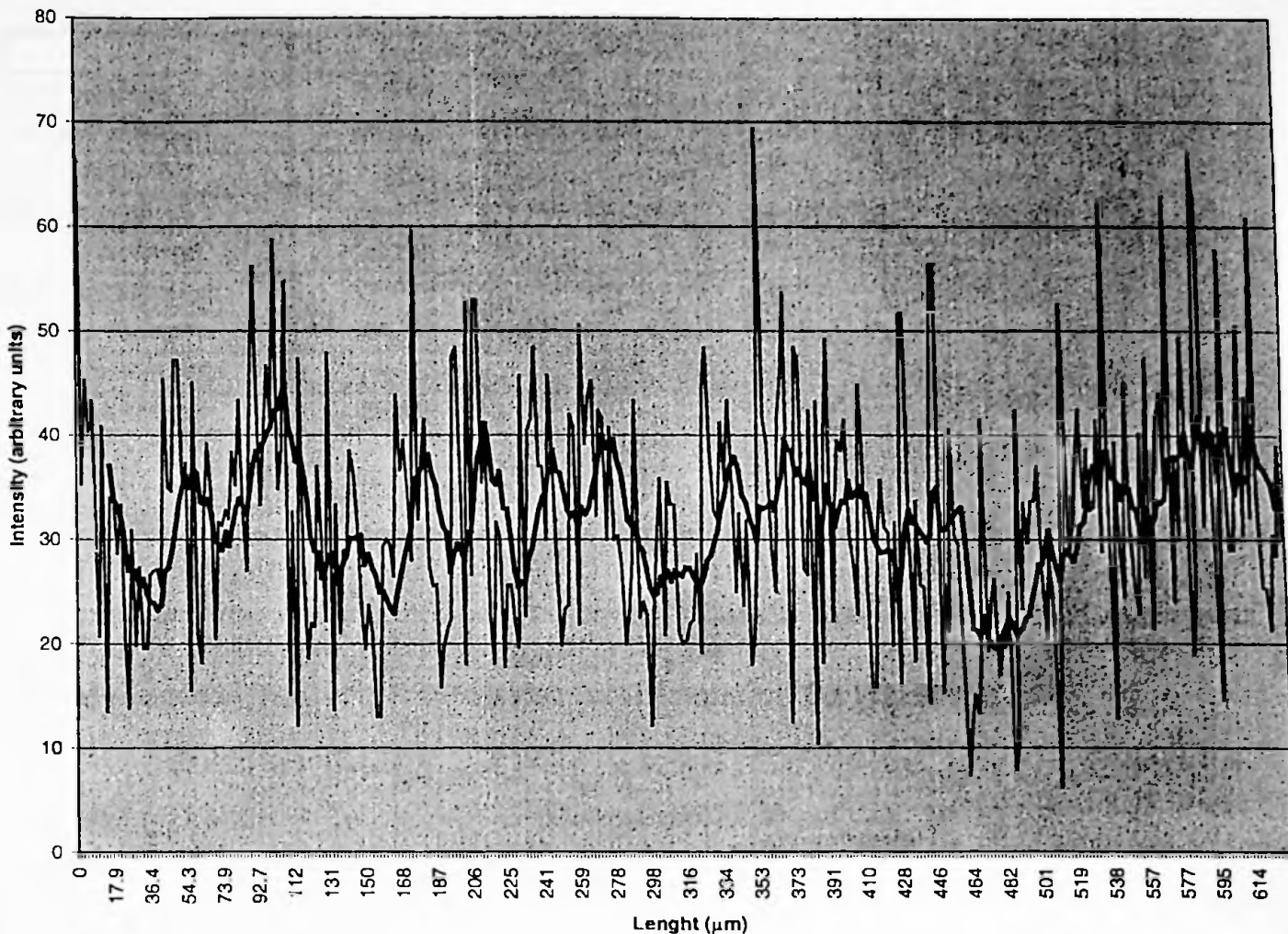


Figure 39. Line Intensity of Sample M. (Light line = raw data) (Dark line = 10 point moving average)

The line intensity graph does not show the distinct drop in intensity between the patterns and the background reflecting the fact that the fluorescence of the pattern is not intense as that seen in long term exposures. The average intensity of the graph is not very high and the maximum intensity is below 70, reflecting the low contrast of the patterns.

Table 7 presents the calculated average intensity of the pattern and the background. The signal to background ratio is 1.3.

Table 11. Average Intensities of Sample M

	Avg. Intensity	Length Interval
First patterns	33.795	3.354-108.212
Second patterns	33.885	165.875-267.379
Third patterns	33.292	355.347-454.479
Fourth patterns	36.975	522.61-615.611
Average	34.487	
First background	26.128	109.889-155.406
Second background	29.358	274.781-348.927
Third background	24.462	462.576-516.886
Average	26.649	

Comparison of these results with those obtained from Samples I, K, and L further supports the proposed role of sputtered nickel oxide in contributing to the fluorescence signal observed in all experiments conducted utilizing the nickel mask.

Summary and Conclusion:

As mentioned in Table 1, there are many techniques, which can be used to generate protein patterns. The three major techniques are photoresist, photochemical, and self-assembled monolayer (SAM) technology. Table 1 does not list any electron beam techniques however few do exist.^{25,26} In this thesis two new techniques for producing protein patterns on glass one of which involves electron beam induced sputtering of a nickel mask, the other utilizing electron beam irradiation alone were investigated. Experiments were performed to characterize the efficiency of these two methods. An analysis of the results of these experiments, led to an assignment of observed signal intensity to at least four major mechanisms, electron beam induced glass luminescence (EB) (Sample K), electron induced labeled protein adsorption (PEB) (Sample L), intrinsic NiO luminescence (NiL) (Sample F) and NiO adsorbed labeled protein luminescence

(PNi) (Sample C). The order of relative contributions of these mechanisms to the luminescence is $\text{PNi} \gg \text{NiL} > \text{PEB} > \text{EB}$. The contribution of NiO to protein adsorption is much greater than the contribution of electron beam generated surface hydroxyl groups. This research has shown that even though protein patterns can be produced by electron beam direct write onto prepared glass surfaces, more distinct protein patterns can be prepared using a nickel mask.

Future Experiments:

Now that proteins may be patterned on a micro-scalar level using electron beam sputtering of a nickel mask, further experiments using the protein arrays may be performed. One experiment would involve growing single cells on islands of patterned laminin. Once nearby cells outgrow their confinement, they will form junctions with one another. If the junction forming molecules within the cells are tagged with a fluorescent probe, their movements may be tracked with the confocal microscope. For example, S-laminin may be tagged with green fluorescent protein (GFP) and its movement may be monitored with a fluorescence microscope. It is speculated that S-laminin density increases at the point of cell to cell junctions.

In this thesis, patterns were created using a mask with 90- μm circular holes in a hexagonal array. Masks with different sizes and shapes of holes may be used to make protein patterns as desired. The maskless technique may be used to reduce the size of the patterns depending on the magnification limits of the SEM used. Also with the maskless technique, microwriting onto protein and other substrates is possible.

Appendix A:

Dosage Formulas:

Dose = (Current * Time) / Area

Area = 1 / (Magnification)²

DACTA Programs:

The following are standard programs to move the stage in different directions
(power is always set at :p = 8):

1. To go south:

to s

tto "Y setright set power :p onfor 7

end

2. to go east:

to e

tto "X setleft setpower :p onfor 7

end

3. To go west:

to w

tto "X setright set power :p onfor 7

end

Making A Matrix:

This program will make a matrix of points (10X10) with varying beam dwell times of 0.1 sec, 0.5 sec, 1 sec, 5 sec, 10 sec, 15 sec, 30 sec, 60 sec and 5 min blockers at each side of the matrix were used to define the boundaries of the matrix.

to matrix

```
repeat 5 [ e wait 3000 e wait 1 e wait 5 e wait 10 e wait 50 e wait 100 e wait 150
e wait 300 e wait 600 e wait 3000 s wait 3000 w 600 w 300 w 150 w wait 100 w wait 50
w wait 10 w wait 5 w wait 1 w wait 3000 s wait 3000]
end
```

Making Matrix1:

This program will make a matrix of rectangular points (10X10) with the ability to define the same dwell time for each point.

to matrix1

```

repeat 5 [ wait :t e wait :t e wait :t e wait :t e wait :t e wait :t e wait :t e
wait :t e wait :t s wait :t w wait :t w wait :t w wait :t w wait :t w wait :t w wait :t w wait :t
w wait :t w wait :t s]

end

```

Making Matrix2:

This program will make a matrix of rectangular points (9X6) with varying dwell times of 0.5 sec, 0.98 sec, 5 sec, 10 sec, 15 sec, 30 sec, 60 sec, and 5 min blockers at each side of the matrix were used to define the boundaries of the matrix.

to matrix2

```

repeat 3 [ wait 3000 e wait 5 e wait 9.8 e wait 50 e wait 100 e wait 150 e wait 300 e wait
600 e wait 3000 s wait 3000 w 600 w 300 w 150 w wait 100 w wait 50 w wait 9.8 w wait
5 w wait 3000 s]

end

```


References:

1. Pope, N.M., Kulcinski, D.L., Hardwick, A., Chang, Y.-A., *Bioconjugate Chem.*, **1993**, 4, 166-171.
2. Nelson, J.M., Griffin, E.G. *J. Am. Chem. Soc.* **1916**, 18, 1109.
3. Stenesh, J., Dictionary of Biochemistry, John Wiley & Sons, Inc., New York, 1975, 163.
4. Blawas, A.S., Reichert, W.M. *Biomaterials*, **1998**, 19, 595-609.
5. MacAlear, J., Wehrung, J., US Patent: 4,103,073. 1978.
6. Lom, B., Healy, K.E., Hockberger, P.E., *J. Neurosci. Methods*, **1993**, 50, 385-397.
7. Ingber, D.E., Whitesides, G.M., Chen, C.S., Mrksich, M., Huang, S., *SCIENCE*, **1997**, 276, 1425-1428.
8. Anderson, K. N., Anderson L. E., Glanze, W. D., *Mosby's Dictionary*, Mosby-Year Book, Inc., Missouri, **1994**, 88.
9. Whitesides, G.M., Lopez, G.P., Biebuyck, H.A., Harter, R., Kumar, A., *J. Am. Chem. Soc.* **1993**, 115, 10774-10781.
10. Bhatia, S.K., Shriver-Lake, L.C., Prior, K.J., Georger, J.H., Calvert, J. M., Bredehorst, R., Ligler, F.S., *Anal. Biochem.*, **1989**, 229, 169-76.
11. Kleinfeld, D., Kahler, K. H., Hockberger, P.A., *Neurosci.*, **1988**, 8 (11), 4098-120.
12. Sigrist H., *Optic Eng.*, **1998**, 34(8), 2339-48.
13. Singhvi, R., Kumar, A., Lopez, G.P., Stephanopoulos, G.N., Wang, D.I.C., Whitesides, G.M., Ingber, D.E. *Science*, **1994**, 264, 696-8.
14. Sanes, J.R., Hunter, D.D., Green, T.L., Merlie, J.P. *Cold Spring Harbor symp. Quant. Biol.* **1990**, LV, 419-430.

15. Lodish, H., Baltimore, D., Berk, A., Zipursky, S.L. *Molecular Cell Biology*, Scientific American Books, Inc., New York, **1995**, 1124-1144.
16. Iwamoto, Y., Robey, F.A., Graf, J., Sasaki, M., Kleinman, H.K., Yamada, Y., Martin, G.R. *Science*, **1987**, 238, 1132-1134.
17. Timpl, R. *J. Biol. Chem.*, **1979**, 254, 9933-9937.
18. Kleinmann, H.K. *Biochemistry*, **1982**, 21, 6188-6193.
19. Jolly, W.L. *Modern Inorganic Chemistry*, McGraw-Hill, Inc., New York, **1984**, 320.
20. Goldstein, J.I., Romig, A.D., Newbury, D.E., Lyman, C.E., *Scanning Electron Microscopy and X-Ray Microanalysis*, Plenum Press, New York, **1992**, 31-146.
21. Matsumoto, B., *Methods in Cell biology*, Academic Press, Inc., New York, vol. 38, **1993**.
22. Ege, S. *Organic Chemistry*, D.C. Heath and Company, Third edition, Massachusetts, **1994**, 67.
23. Ballard, C.C., Broge, E.C., Iler, R.K., St. John, D.S., McWhorther, J.R. *J. Phys. Chem.*, **1961**, 65, 20-25.
24. Diaz-Guerra, C., Remon, A., Garcia, J.A., Piqueras, J. *phys. Stat. Sol.*, **1997**, 167, 497-503.
25. Ahn, C. H., Tybell, T., Antoganzza, L., *SCIENCE*, **1997**, 276, 1100-1103.
26. Bergman, A.A., Buijs, J., Herbg, J., Mathes, D.T., *Langmuir*, **1998**, 14, 6785-6788.